Ultrawide spectral broadening and compression of single extremely short pulses in the visible, uv-vuv, and middle infrared by high-order stimulated Raman scattering

V. P. Kalosha and J. Herrmann
Max Born Institute for Nonlinear Optics and Short Pulse Spectroscopy, Max-Born-Straße 2a, 12489 Berlin, Germany
(Received 30 January 2003; published 28 August 2003)

We present the results of a comprehensive analytical and numerical study of ultrawide spectral broadening and compression of isolated extremely short visible, uv-vuv and middle infrared (MIR) pulses by high-order stimulated Raman scattering in hollow waveguides. Spectral and temporal characteristics of the output pulses and the mechanism of pulse compression using dispersion of the gas filling and output glass window are investigated without the slowly varying envelope approximation. Physical limitations due to phase mismatch, velocity walk off, and pump-pulse depletion as well as improvements through the use of pump-pulse sequences and dispersion control are studied. It is shown that phase-locked pulses as short as ~ 2 fs in the visible and uv-vuv, and 6.5 fs in the MIR can be generated by coherent scattering in impulsively excited Raman media without the necessity of external phase control. Using pump-pulse sequences, shortest durations in the range of about 1 fs for visible and uv-vuv probe pulses are predicted.

DOI: 10.1103/PhysRevA.68.023812 PACS number(s): 42.65.Dr, 42.65.Re

I. INTRODUCTION

In the last decade ultrafast laser technology has been developed rapidly and successfully applied to a large variety of fields, especially for time-resolved studies of fast-evolving fundamental physical and chemical processes. Three main ingredients of this technological advance are connected with the development of Kerr-lens mode-locked solid-state lasers, chirped pulse amplification and extracavity compression techniques [1,2]. The traditional method for pulse compression is based on the Kerr nonlinearity in waveguides to produce spectral broadening by self-phase modulation (SPM) and subsequent chirp compensation by anomalous dispersion in carefully designed linear optical elements such as prism pairs, chirped mirrors, or spatial light modulators. Pulses down to 5 fs were generated using single-mode fibers [3] and 4.5 fs by hollow fibers filled with a noble gas [4]. Though the theoretical limit of the bandwidth which can be achieved by this method allows still shorter pulses [5,6], the experimental results obtained to date by this method are difficult to improve practically due to problems in chirp compensation over an extremely broad spectrum and the onset of instabilities for too high input intensities due to plasma generation by ionization. Note that the method of pulse compression by SPM is only applicable in the near-IR and optical range.

There is also a great interest in an efficient pulse compression method in uv and vuv as well as in middle infrared (MIR) for ultrafast time-resolved measurements in material science, chemistry, and biology, where the methods known up to now suffer from low efficiency and too long pulse durations. Numerous applications demand methods for the generation of shorter pulses in optical as well in uv-vuv and MIR and also in the soft x-ray spectral range. Recently, two complementary approaches were studied to push the duration of pulses to shorter limits in different spectral ranges and with different characteristics. On the one hand, high-order harmonic generation of fs pulses [7,8] was shown to be source of trains of attosecond x-ray pulses separated by half of the laser period [9–12]. Reference [13] predicted that single x-ray attosecond pulses required in most applications can be generated from few-cycle laser pulses. Using a new measurement technique recently, attosecond trains [14] as well as single attosecond x-ray pulses [15] have been demonstrated. Based on this progress, first time-resolved spectroscopic measurements in the attosecond domain have been reported in Ref. [16].

In a second approach, high-order stimulated Raman scattering (HSRS) was studied with the aim to generate ultrabroadband spectra with high conversion efficiency sufficient for subfemtosecond pulses. Two different schemes were considered for extremely short pulse generation. Reference [17] theoretically predicted that high-repetition trains of subfemtosecond pulses can be obtained using adiabatic excitation of the medium by a properly detuned two-color cw field. Recently this technique was experimentally demonstrated in Ref. [18].

In another much promising scheme, impulsive excitation by ultrashort pulses and a pump-probe arrangement is used to compress a probe pulse by the Raman medium excited by the pump pulse. Using such an arrangement in Refs. [19,20], the first experimental demonstration of pulse compression by HSRS was reported with the generation of a train of 6-fs pulses. A mechanism for the generation of single compressed pulses by HSRS for probe pulses shorter than the period of Raman oscillations was first proposed and theoretically studied in Refs. [21,22], predicting compression of single pulses without additional chirp control caused by the material dispersion of the medium itself. This regime was used to produce the shortest single optical pulses with a duration of 3.8 fs in SF_6 [23]. There exist a number of additional studies of pulse compression by HSRS. The use of strong-field alignment combined with shaped-pulse optimization for efficient rotational wave-packet excitation was proposed in Ref. [24]. Probe-pulse compression by rotational wave packets in CO_2 was demonstrated in Ref. [25]. The regime of adiabatic two-color excitation was studied in Refs. [26–28], and in Refs. [29–31] a combination of the adiabatic regime with the

pump-probe regime was considered. Before, pulse compression by HSRS was discussed in Ref. [32], using the assumption that all spectral lines generated by HSRS have equal phases. However, it was found in Ref. [21] that the Raman lines are not phase locked but different lines show phase jumps of π. There exist also other proposals to use phase locking by multicomponent Raman solitons [33] or to compress pulses by the use of plasma wakefields [34].

Optical excitation of coherent molecular vibrations or rotations via stimulated Raman scattering has mainly been carried out in one of the three ways. The original method consists of focusing of an intense pump field with carrier frequency ω_{pu} into a Raman medium where, due to the two-photon stimulated process, a Stokes wave with frequency $\omega_{pu}-\Omega$ is generated, growing out from spontaneous Raman emission where Ω is the Raman frequency shift (see, e.g., Refs. [35,36]). This process may be observed if the laser intensity exceeds a certain threshold. Anti-Stokes radiation often appears on a cone determined by the phase-matching condition. The second method which is possible in a collinear setup is to excite the Raman medium by two tunable laser outputs with frequencies ω_{pu} and $\omega_{pu}-\Omega$ (two-color excitation) [37], which are adjusted to match the Raman frequency Ω. Coherent Raman excitation can also be achieved using a third method, the impulsive technique [38,39], in which a single ultrashort pulse with duration shorter than the Raman oscillation period $T_R=2\pi/\Omega$ initiates the coherent vibrational or rotational motion. Then the spectral width exceeds the Raman shift and stimulated Raman scattering occurs through mixing among frequency components contained within the pulse bandwidth. In the impulsive regime the vibrational amplitudes of Raman excitation can be increased by using synchronized pulse sequences [40].

The last two methods do not involve a laser intensity threshold and for appropriate conditions they can be used for the aim of pulse compression to extremely short durations, because multiple Raman lines are generated in collinear direction after a certain propagation length by HSRS. The process of HSRS has been known for many years [41,42]. If only a single long pump beam is launched into the medium, multiple nonphasematched Stokes lines arise in collinear direction as a cascaded process where the lower-order Stokes lines undergo a rapid depletion to drive the next order in the line sequence [35,36]. This means that in this case all the energy is essentially contained in the highest Stokes order. An early theoretical study of HSRS in the framework of the slowly varying envelope approximation (SVEA) is presented in Ref. [43] which shows a distribution of the spectral lines described by Bessel functions. In the case of two-color excitation with a pump and a first Stokes pulse of comparable intensities, a large number of Stokes and anti-Stokes lines are generated in collinear direction spanning the range from IR to uv [26,37,44–48]. Theoretical studies of this regime were published in Refs. [43,49–52]. Multiple Raman lines have also been observed in the impulsive pump-probe regime [53,54]. In Refs. [21,22] we predicted that for probe pulses with a duration smaller than the period of Raman oscillations, the HSRS spectrum becomes continuous with ultrabroadband width.

The present paper extends our previous papers [21,22,55,56] and contains the results of a comprehensive investigation of pulse compression by HSRS studying a number of additional issues. In Sec. II, the basic propagation equation is derived for the description of ultra-broad HSRS without standard approximations as the use of SVEA and a Taylor expansion for the dispersion. In Sec. III, the specific character of HSRS is investigated by analytical solutions of the basic equations. The derived exact analytical solution of the reduce Maxwell equation shows that the interesting features of ultrawide spectral broadening by HSRS cannot be described with the help of the SVEA. In Sec. III B, analytical expressions for the spectral phases, the spectrum, and the ultimate shortest pulse durations are derived from the analytical solution. This allows one to reveal the main physical specifics of phase-amplitude modulation and pulse compression by HSRS, as the behavior of the spectral phases, the accessible bandwidths, the possibility to compress pulses by normal dispersion simply by a piece of glass, but also by anomalous dispersion, and specific features for a probe-pulse delay near the out-of-phase point of Raman oscillations, where the Fourier-transformed field is real but changes the sign, i.e., the spectral phase jumps from zero to π inside the spectrum. The possibility to compress such pulses with phase jumps by smooth normal dispersion demonstrates a kind of pulse compression not known up to now in ultrafast optics by separation of the pulse into a short bandwidth-limited and a long phase-modulated pulse. Compression of chirped probe pulses, the generation of trains for probe pulses much longer than T_R, the partial influence of phase mismatch, walk-off effects, and the limit of small Raman modulation described by the SVEA are discussed in Secs. III D, III E, III F, and III G, respectively. In Sec. IV, numerical solutions are presented for pulse compression in the optical range, which takes into account the full influence of dispersion and the change of the pump by HSRS during propagation in the Raman medium. In particular, the influence of dispersion is studied and optimum conditions are found with compression up to 1.7 fs in SF_6. Choosing the same parameters as in Ref. [23] the results show good agreement with corresponding experimental observations. In Sec, IV B, the pump regime with a sequence of pulses is considered with the aim to increase the Raman amplitude, and pulse compression in the optical range up to about 1 fs is predicted. In Sec. V, the compression of extremely short uv-vuv pulses with the use of pulse sequences and dispersion control by pressure optimization and in Sec. VI, that of MIR pulses are studied. Using such optimization we predict compression of initial 70-fs pulses at wavelengths from 400 nm to 160 nm to about 1 fs and at 4 μm to about 6.5 fs in *para*-H_2.

II. THEORETICAL FUNDAMENTALS

The standard theoretical method in nonlinear optics is the slowly varying envelope approximation (SVEA), in which the rapidly varying part of the electric field $\mathbf{E}(\mathbf{r},t)$ propagating in the z direction is separated from the slowly varying envelope $\mathbf{A}(\mathbf{r},t)$ with the help of the following ansatz (see, e.g., Ref. [35]):

$$\mathbf{E}(\mathbf{r},t)=\frac{1}{2}\mathbf{A}(\mathbf{r},t)\exp[i\omega_0 t-k(\omega_0)z]+\text{c.c.}, \tag{1}$$

where ω_0 is the input carrier frequency, $k(\omega)=\omega n(\omega)/c$ is the wave number, and $n(\omega)$ is the frequency-depending refractive index. In the SVEA the slowly varying envelope is assumed to satisfy the conditions

$$\left|\frac{\partial \mathbf{A}}{\partial t}\right| \ll \omega_0|\mathbf{A}|, \tag{2a}$$

$$\left|\frac{\partial \mathbf{A}}{\partial z}\right| \ll k(\omega_0)|\mathbf{A}|. \tag{2b}$$

Equation (2a) is fulfilled only if the spectral width of a pulse $\Delta\omega$ is much smaller than the carrier frequency ω_0 of the pulse: $\Delta\omega \ll \omega_0$. It allows one to neglect higher-order terms in the Taylor expansion of $k(\omega)$ around ω_0. In general, it is obvious that the approximation (2a) (SVEA in time) and the Taylor expansion are no longer valid for radiation with ultrawide spectra, such as pulses with duration approaching one optical cycle, while the approximation (2b) (SVEA in space) is much less restrictive. Therefore, the SVEA in time cannot be used for conditions studied here.

Nonlinear pulse propagation without special prerequisites of the SVEA can be studied by the numerical solution of Maxwell equations by the finite-difference time-domain method [57] along with solutions for the material equations (see Refs. [5,58,59] and references therein). However, the large numerical effort of this approach, which directly resolves high optical oscillations of the field, both in time and space, limits possible propagation lengths to a few mm. In several papers various improved approximated equations have been derived, which allow the theoretical description beyond the validity of the standard approach [2,60,61]. In the following, we give a systematic derivation of a more general first-order unidirectional propagation equation in three-dimensions (3D), without the use of the SVEA in time and the Taylor expansion of the linear refractive index which includes vectorial effects and is valid both for isotropic and anisotropic media without spatial dispersion. This equation generalizes the previously derived equations into the nonparaxial and extremely nonlinear region from which the basic equations of Refs. [60,61] can be derived by straightforward approximations.

The propagation of the optical pulses in nonlinear media is described by the following wave equation [62]:

$$\left(\frac{\partial^2}{\partial z^2}+\Delta_\perp\right)\mathbf{E}-\boldsymbol{\nabla}(\boldsymbol{\nabla}\cdot\mathbf{E})-\frac{1}{c^2}\frac{\partial^2 \mathbf{E}}{\partial t^2}=\mu_0\frac{\partial^2 \mathbf{P}}{\partial t^2}, \tag{3}$$

and Gauss's law

$$\boldsymbol{\nabla}\cdot\mathbf{E}=-\frac{1}{\epsilon_0}\boldsymbol{\nabla}\cdot\mathbf{P}, \tag{4}$$

where $\Delta_\perp$ is the transverse Laplacian and $\mathbf{P}=\mathbf{P}_\mathrm{L}+\mathbf{P}_\mathrm{NL}$ is the medium polarization with linear nonresonant contributions $\mathbf{P}_\mathrm{L}$ and nonlinear or resonant (as, e.g., given by the Raman effect) contributions $\mathbf{P}_\mathrm{NL}$. The z direction is marked out here because we suppose later a predominant propagation in this direction but without the assumption of the paraxial approximation. Substituting the Fourier-transformed field

$$\mathbf{E}(\mathbf{k}_\perp,z,\omega)=\int_{-\infty}^{\infty}\mathbf{E}(\mathbf{r},t)\exp(i\mathbf{k}_\perp\mathbf{r}_\perp-i\omega t)d\mathbf{r}_\perp dt \tag{5}$$

and analogous expression for the polarization $\mathbf{P}(\mathbf{r},t)$ into Eq. (3), for the transverse component of the electric field $\mathbf{E}_\perp=\{E_x,E_y\}$, we can rewrite the wave equation in the form

$$\left(\frac{\partial^2}{\partial z^2}+h_j^2\right)E_j(\mathbf{k}_\perp,z,\omega)=0 \tag{6}$$

with

$$h_j^2(\mathbf{k}_\perp,z,\omega)=\frac{\omega^2}{c^2}-\mathbf{k}_\perp^2+\frac{ik_j\tilde{\nabla}\cdot\mathbf{E}+\mu_0\omega^2 P_j}{E_j}. \tag{7}$$

Here $\tilde{\nabla}\cdot\mathbf{E}=-i\mathbf{k}_\perp\mathbf{E}_\perp+\partial E_z/\partial z$, $j=\{x,y\}$ and the Fourier-transformed linear polarization $\mathbf{P}_\mathrm{L}(\mathbf{k}_\perp,z,\omega)=\epsilon_0\hat{\chi}(\omega)\mathbf{E}(\mathbf{k}_\perp,z,\omega)$, where $\hat{\chi}(\omega)$ is the linear susceptibility tensor of the anisotropic medium. Equations (6) and (7) obviously describe coupling of different components of the electric field due to the linear and nonlinear polarizations as well as due to the vector character of Maxwell equations related to the $\boldsymbol{\nabla}\cdot\mathbf{E}$ term in Eq. (3). Because of the two latter factors a mixture of different components of the electric field arises even in an isotropic medium.

In most typical situations the condition

$$\partial h_j/\partial z \ll h_j^2 \tag{8}$$

is satisfied even if the condition (2b) is not fulfilled. Therefore, the separation $\partial^2/\partial z^2+h_j^2=(\partial/\partial z-ih_j)(\partial/\partial z+ih_j)$ is possible. The electric field can be split into a forward $\mathbf{E}^+$ and a backward $\mathbf{E}^-$ propagating parts: $\mathbf{E}(\mathbf{k}_\perp,z,\omega)=\mathbf{E}^+(\mathbf{k}_\perp,z,\omega)+\mathbf{E}^-(\mathbf{k}_\perp,z,\omega)$. Let us consider a pulse propagating only in forward direction along the z axis, $E_j^+\propto\exp[ik(\omega_0)z]E_j^{(0)}(\mathbf{k}_\perp,z,\omega)$, and neglect waves propagating backward. This requires that the linear refractive index is a smooth, slowly changing function of the z coordinate. Therefore, from Eq. (6) we have

$$\frac{\partial E_j^+}{\partial z}=ih_jE_j^+, \tag{9}$$

where the backward wave in expression (7) is neglected. From Eq. (4) we have

$$\frac{\partial E_z^+}{\partial z}=i\mathbf{k}_\perp\cdot\mathbf{E}_\perp^+-\frac{1}{\epsilon_0}\left(-i\mathbf{k}_\perp\mathbf{P}_\perp^+\frac{\partial P_z^+}{\partial z}\right). \tag{10}$$

Note that the right-hand side term $h_jE_j^+$ in Eq. (9) has no singularity for $E_j^+\to 0$.

Equations (9) and (10) are first-order evolution equations in 3D without SVEA, paraxial approximation or perturbative

inclusion of vectorial effects, and valid for isotropic and anisotropic media with an arbitrary functional form for the nonlinear polarization. They can be solved numerically as a boundary problem by the split-step operator method [63]. They take into account a possible extremely broad bandwidth, sharp temporal features, and nonaxial effects in space-time coupling, higher-order nonlinear and dispersive and also vectorial and anisotropic effects. Note that the SVEA with paraxial approximation for the transverse momentum and neglect of vectorial effects fails to describe accurately self-focusing in dispersive media long before the temporal structure reaches the time of an optical cycle [64–66].

Equations (9) reduce tremendously the numerical effort in solving the exact three-dimensional Maxwell equations. In general, the full three-dimensional integration of the exact Maxwell equation for propagation lengths in the range of tens of cm is outside the capacity of computers available today. The only approximation here is the assumption of weak backward waves and the requirement expressed by the relation (8), both of which are only very weak restrictions. The relation (8) can be written as $\partial \Delta n_{\mathrm{NL}}(E)/\partial z \ll k(\omega_0)$, where Δn_{NL} is defined by $P_{\mathrm{NL}}=\varepsilon_0 \Delta n_{\mathrm{NL}} E$. This is a much weaker condition than the condition (2b) required for the approximate evolution equations derived below. The scalar variant of Eqs. (9) was derived by one of the authors in Ref. [67]. For the aim of the present work it is not necessary to use the full capacity of Eqs. (9) and (10); they will be applied in forthcoming work.

Previously derived evolution equations without SVEA as presented in Refs. [2,61] can be derived from Eqs. (9). Introducing the refractive index $n^2(\omega)=1+\chi(\omega)$ for an isotropic medium $\nabla \cdot \mathbf{E}=0$ and assuming small contribution of the beam's nonparaxiality as well as nonlinearity, we expand the square root in Eq. (7) as

$$h_j \approx k(\omega) - \frac{\mathbf{k}_\perp^2}{2k(\omega)} + \frac{\mu_0 \omega^2 (P_{\mathrm{NL}})_j}{2k(\omega) E_j}. \tag{11}$$

Then we introduce the moving time coordinate $\eta = t - z/c$, make the substitution $\partial/\partial z \to \partial/\partial z - \partial/c\partial\eta$, and after back Fourier transformation to the real spatial coordinates from Eqs. (9) we obtain the following basic equation [61]:

$$\frac{\partial \mathbf{E}_\perp(\mathbf{r},\omega)}{\partial z} = \frac{i\omega}{c}[n(\omega)-1]\mathbf{E}_\perp(\mathbf{r},\omega) + \frac{i}{2k(\omega)}\Delta_\perp \mathbf{E}_\perp(\mathbf{r},\omega) + \frac{i\mu_0\omega^2}{2k(\omega)}\mathbf{P}_{\mathrm{NL}}(\mathbf{r},\omega), \tag{12}$$

where, here and below, the superscript "+" is omitted.

In a bulk medium the nonuniform transverse intensity profile of the beam leads to nonuniform phase relations due to diffraction and nonlinear transverse reshaping effects. Pulse compression by SPM or HSRS in a nonlinear bulk medium is therefore substantially limited. A possible solution of this problem is using hollow fibers filled with a gas as nonlinear medium. This technique was first applied for optical pulse compression by self-phase modulation using hollow-core silica waveguides filled with a noble gas [2,4,68]. The same technique was also used for impulsive Raman scattering with a Raman-active gas as H_2 or SF_6 [19,20,53].

For the description of wave propagation in hollow fibers the electric field in frequency domain can be separated into a longitudinal and a transverse part $\mathbf{E}_\perp(\mathbf{r},\omega) = \mathbf{F}(\mathbf{r}_\perp,\omega)\tilde{E}(z,\omega)$, where the transverse distribution $\mathbf{F}(\mathbf{r}_\perp,\omega)$ is the solution of the Helmholtz equation

$$[\Delta_\perp + k^2(\omega)]\mathbf{F} = \beta^2(\omega)\mathbf{F}, \tag{13}$$

with the eigenvalue $\beta(\omega)$ for the fundamental mode. Then the longitudinal distribution $\tilde{E}(z,\omega)$ satisfies the equation

$$\frac{\partial \tilde{E}}{\partial z} = i\left(\beta - \frac{\omega}{c}\right)\tilde{E} + \frac{i\mu_0\omega^2\alpha}{2k(\omega)} P_{\mathrm{NL}}(z,\omega). \tag{14}$$

Here $\alpha=\alpha(\omega)$ is the nonlinearity reduction factor depending on the nonlinearity of the medium. In the case of third-order nonlinear effects $\alpha = \int_S F^4(\mathbf{r}_\perp)\mathrm{d}\mathbf{r}_\perp / S_1$, $S_1 = \int_S F^2(\mathbf{r}_\perp)\mathrm{d}\mathbf{r}_\perp$ being the effective mode area and S being the cross-section of the fiber.

Equation (14) is a generalization of the so-called *reduced* Maxwell equation [60] which is valid only for a refractive index close to unity. The reduced Maxwell equation is obtained from Eq. (12) by the substitution $n(\omega)-1 \approx [n^2(\omega)-1]/2$ and back Fourier transformation into the time domain:

$$\frac{\partial E}{\partial z} = -\frac{\mu_0 c}{2}\frac{\partial P}{\partial \eta}. \tag{15}$$

This equation is a useful tool for examining the nonlinear effects of ultrabroadband radiation in gaseous media. It was recently applied for the study of pulse compression and supercontinuum generation by the optical Kerr effect [6] and by high-order stimulated Raman scattering [21,22] in hollow waveguides. However, for solids the solutions of this equation differ from the exact Maxwell equation as was shown in Ref. [67].

The Fourier-transformed linear polarization is given by

$$P_{\mathrm{L}}(z,\omega) = \epsilon_0[\chi_{\mathrm{b}}(\omega) + \chi_{\mathrm{g}}(\omega)]E(z,\omega), \tag{16}$$

where χ_{b} is the bulk susceptibility defined by the Sellmeyer formula $\chi_{\mathrm{b}}(\omega) = \Sigma_\ell S_\ell/(\omega_\ell^2 - \omega^2)$ with experimentally determined parameters S_ℓ, ω_ℓ. The solution of Eq. (13) for the transverse-mode distribution of a dielectric hollow waveguide with mode diameter much larger than the wavelength was found by Marcatili and Schmelzer [69]. For the hollow waveguide with radius $R \gg \lambda$, the waveguide contribution for the fundamental EH_{11} mode is given by $\chi_{\mathrm{g}}(\omega) = (2.405c/\omega R)^2[1 + i(1+\nu^2)/(2\pi R\sqrt{1-\nu^2})]$, where $\nu \simeq 1.45$ is the ratio between the refractive indices of fused silica and the internal gas.

For the description of the Raman effect we assume that only two rotational or vibrational levels are excited by the pump pulse. This assumption is justified if the Raman frequency is not too small, as, e.g., in H_2 or SF_6. The Raman

polarization $P_R = N\mathrm{Sp}(\hat{\alpha}\hat{\rho})E$ then can be described by the two-photon two-level system equations (see, e.g., Ref. [70]):

$$\left(\frac{\partial}{\partial\eta}+\frac{1}{T_2}-i\Omega\right)\rho_{12}=\frac{i}{2\hbar}[(\alpha_{11}-\alpha_{22})\rho_{12}+\alpha_{12}w]E^2, \tag{17a}$$

$$\frac{\partial w}{\partial\eta}+\frac{w+1}{T_1}=\frac{i\alpha_{12}}{2\hbar}(\rho_{12}-\rho_{12}^*)E^2, \tag{17b}$$

where $\rho_{12}=\frac{1}{2}(u+iv)$, $w=\rho_{22}-\rho_{11}$, $\hat{\rho}$ is the density matrix, $\hat{\alpha}$ is the two-photon polarizability matrix responsible for the Raman process and Stark shift, Ω is the Raman frequency shift, N is the density, and T_1 and T_2 are the relaxation times. Note that the two-level model can not be applied for molecules with small rotational frequencies (e.g., for N_2 or CO_2) in which a pump pulse induces rotational wave packets with a nonsinusoidal Raman excitation. In this case different models can be used for the theoretical description, as the multilevel density matrix or the solutions of the simplified Schrödinger equation [24], but the analysis of rotational wave-packet excitation is outside the scope of the present paper.

The generation of multiple Stokes and anti-Stokes Raman lines by HSRS is described in many works [17,27,28,35,36,43,49–52] in the frequency domain using the SVEA and the rotating wave approximation by a spectral decomposition $E(z,t)=\frac{1}{2}\Sigma_l A_l(z,t)\exp[i(k_l z-\omega_l t)]+\mathrm{c.c.}$ with $\omega_l=\omega_0+l\Omega$, $k_l=\omega_l n(\omega_l)/c$, $(l=0,\pm1,\ldots)$, the pump carrier frequency ω_0 and the complex slowly varying envelopes A_l. Then using the condition (2) from the wave equation (3) the following coupled equations can be derived:

$$\frac{\partial A_l}{\partial z}+\frac{1}{v_l}\frac{\partial A_l}{\partial t}=-\frac{i\mu_0 c\omega_l}{2n(\omega_l)}P_l, \tag{18}$$

where $v_l=(dk_l/d\omega_l)^{-1}$ is the group velocity of the spectral component ω_l and P_l is the polarization which describes the interaction of different spectral components ω_l and is given by

$$P_l=\frac{1}{2}N[\alpha_{12}(\tilde{\rho}_{12}e^{i\Delta_{l+1}z}A_{l+1}+\tilde{\rho}_{12}^*e^{-i\Delta_l z}A_{l-1}) +(\alpha_{11}\rho_{11}+\alpha_{22}\rho_{22})A_l], \tag{19}$$

where $\Delta_l=k_l-k_{l-1}$ is the phase mismatch in the axial direction and $\tilde{\rho}_{12}=\rho_{12}\exp[-i(\omega_0-\omega_S)\eta]$. For the slowly varying density matrix element $\tilde{\rho}_{12}$ the following equation can be found from Eq. (17a):

$$\frac{\partial\tilde{\rho}_{12}}{\partial\eta}+\left(i\Delta+\frac{1}{T_2}\right)\tilde{\rho}_{12}=i\Theta w, \tag{20}$$

with $\Delta=\omega_0-\omega_S-\Omega+(\alpha_{22}-\alpha_{11})\Sigma_l|A_l|^2/8\hbar$, $\Theta=\alpha_{12}\Sigma_l A_l A_{l-1}^*\exp(i\Delta_l z)/8\hbar$.

To compare Eq. (18) in SVEA with the reduced Maxwell equation (15), we substitute the same spectral decomposition for the field into Eq. (15) and come to the following result:

$$\frac{\partial A_l}{\partial z}+\left(\frac{1}{v_l}+b_l\right)\frac{\partial A_l}{\partial t}+a_{l+1}\frac{\partial A_{l+1}}{\partial t}+a_l^*\frac{\partial A_{l-1}}{\partial t} =-\frac{i\mu_0 c\omega_l}{2n(\omega_l)}P_l, \tag{21}$$

where $a_{l+1}=\frac{1}{4}\mu_0 cN\alpha_{12}\tilde{\rho}_{12}\exp(i\Delta_{l+1}z)/n(\omega_l)$ and $b_l=\frac{1}{4}\mu_0 cN(\alpha_{11}\rho_{11}+\alpha_{22}\rho_{22})/n(\omega_l)$. The comparison with Eq. (18) shows that in the left-hand side term of Eq. (21), the third and fourth terms describe an additional coupling between different spectral components A_l. As will be shown in Sec. III G, these terms are of crucial importance in the case of a moderate or large Raman gain or a large number of sidebands.

In the case of short-pulse impulsive excitation in a pump-probe regime, the evolution of the pump and the probe pulse can be described more simply in the temporal range by single equations for the amplitudes. Using SVEA, the equation for the probe pulse is given by

$$\frac{\partial A_{pr}}{\partial z}+\frac{1}{v}\frac{\partial A_{pr}}{\partial t}=-i\frac{\mu_0 c\omega_{pr}N\alpha_{12}}{4n(\omega_{pr})}\tilde{\rho}_{12}A_{pr}, \tag{22}$$

where $\tilde{\rho}_{12}$ is determined by Eq. (20) with A_0 as the pump pulse and $A_l=0$ for $l\neq0$. However, the validity of Eq. (22) is also substantially limited to the range of a small spectral broadening and cannot be used for the purposes of the present manuscript.

In the following, we solve the more general evolution Eq. (15), which is valid for ultrawide spectral broadening with a width exceeding the carrier frequency and takes into account all spectral components in a single equation, but also phase mismatch, walk off, high-order dispersion, and pump-pulse depletion. The price for this significant advantage is the necessarily higher resolution of the temporal grid in the scale of the carrier frequency, while in the SVEA equations (18) the resolution is in the scale of the pulse duration. On the other hand, using the split-step Fourier method the necessary spatial resolution for the numerical solution of the wave equation (15) can be chosen much larger than with the finite-difference time-domain method.

III. ANALYTICAL SOLUTION FOR THE IMPULSIVE PUMP-PROBE REGIME

A. General solution

First, we derive an analytical solution of Eqs. (15) and (17a) for the impulsive regime where a short pump pulse with duration

$$\tau_{pu}<T_R=2\pi/\Omega \tag{23}$$

excites the Raman medium and a delayed weaker probe pulse is amplitude and phase modulated due to the long-living molecular excitation of the foregoing pump pulse (see Fig. 1). Then the probe-pulse propagation is in a linear regime with polarization

$$P_R=N\alpha_{12}u(z,\eta)E_{pr}(z,\eta), \tag{24}$$

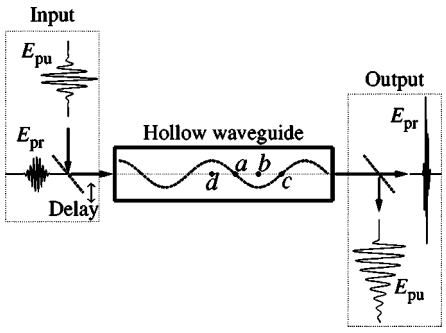

FIG. 1. Schematic diagram of an impulsive pump-probe regime for pulse compression using high-order stimulated Raman scattering in a gas-filled hollow waveguide. The periodic response of the molecular system in hollow waveguide is shown, where the positions of the input probe pulse at the out-of-phase point, minimum, in-phase point, and maximum are indicated by a, b, c, and d, respectively.

where $u(z,\eta)$ depends only on the pump pulse. For rather general situations the medium response for the probe pulse can be presented approximately by the following general separation ansatz:

$$u(z,\eta)=u_0(z)a(\eta), \tag{25}$$

where u_0 is the amplitude of Raman excitation.

The specific form of the function $a(\eta)$ is different for the case of two contributing Raman levels excited impulsively by a short pump pulse, a pulse sequence or two-color long pulses from that of rotational wave packets with the excitation of many lines (see, e.g., Refs. [24,25]) with nonsinusoidal excitation, but the solution given below can be used in both cases. In the case of a two-level Raman medium, the functions $u_0(z)$ and $a(\eta)$ can be calculated in a simple way if relaxation, population changing, and Stark effect can be neglected. Then Eqs. (17) for the density matrix is simplified to the equation

$$\left(\frac{\partial}{\partial\eta}-i\Omega\right)\rho_{12}=-\frac{i\alpha_{12}}{2\hbar}E_{pu}^2. \tag{26}$$

The solution of Eq. (26) for $u=2\mathrm{Re}\rho_{12}$ is given by

$$u(z,\eta)=u_0(z,\eta)\sin[\Omega\eta+\psi(z,\eta)], \tag{27}$$

with

$$u_0=\frac{\alpha_{12}}{\hbar}[b_1^2(z,\eta)+b_2^2(z,\eta)]^{1/2},$$

$$\psi=-\arctan\left(\frac{b_2}{b_1}\right),$$

$$b_1=\int_{-\infty}^{\eta}E_{pu}^2(z,\eta')\cos\Omega\eta'\,d\eta',$$

$$b_2=\int_{-\infty}^{\eta}E_{pu}^2(z,\eta')\sin\Omega\eta'\,d\eta'.$$

As can be shown by numerical solutions (see Sec. IV), for the considered regimes $b_1\ll b_2$ and the phase $\psi(z,\eta)$ is small. For a pump-probe delay much larger than the pump-pulse duration τ_{pu}, we have the separation ansatz (25).

In a gaseous medium the main mechanism of the ultrawide spectral broadening and pulse compression can be understood with the neglect of linear dispersion. Then the propagation equation (15) for the probe pulse $E_{pr}(z,\eta)$ is

$$\frac{\partial E_{pr}}{\partial z}=-\gamma u_0(z)\frac{\partial}{\partial\eta}[a(\eta)E_{pr}], \tag{28}$$

where $\gamma=\frac{1}{2}\mu_0cN\alpha_{12}$. The first-order partial differential equation (28) can be solved using the equations of its characteristics [71] given by

$$\frac{dz}{d\xi}=1, \tag{29a}$$

$$\frac{d\eta}{d\xi}=\gamma u_0(z)a(\eta), \tag{29b}$$

$$\frac{dE_{pr}}{d\xi}=-\gamma u_0(z)\frac{da}{d\eta}E_{pr}. \tag{29c}$$

The solution of Eqs. (29a) and (29b) is

$$z=\xi+z_0, \tag{30a}$$

$$\int_{\eta_0}^{\eta}\frac{d\eta'}{a(\eta')}=\gamma\int_{z_0}^{z}u_0(z')\mathrm{d}z', \tag{30b}$$

and Eq. (29c) can be transformed to

$$\frac{dE_{pr}}{d\eta}=-\frac{1}{a(\eta)}\frac{da}{d\eta}E_{pr}, \tag{31}$$

with the solution

$$E_{pr}=E_{pr}(\eta_0)\frac{a(\eta_0)}{a(\eta)}. \tag{32}$$

Using the initial conditions for $\xi=0$, $z_0=0$, $\eta_0=s$, $E_0=E_{pr}(s)$, where s is the parameter of the characteristic lines, and $E_{pr}(\eta)$ is the input probe-pulse field at $z=0$, we find the solution of Eq. (28) as follows:

$$E_{pr}(z,\eta)=E_{pr}(s)\frac{a(s)}{a(\eta)}, \tag{33a}$$

$$\int_{\eta}^{s}\frac{d\eta'}{a(\eta')}=\gamma\int_{0}^{z}u_0(z')dz'. \tag{33b}$$

From Eqs. (25) and (27) and for $|b_1|\ll|b_2|$ we have $a(\eta)=\sin\Omega\eta$ and the solution for the probe pulse is as follows [21,55]:

$$E_{pr}(z,\eta)=E_{pr}(s-t_m)\frac{\sin\Omega s}{\sin\Omega\eta}, \tag{34}$$

where $E_{pr}(\eta)=A_{pr}(\eta)\cos\Omega_{pr}\eta$ and the initial probe-pulse envelope is chosen here to be the Gaussian: $A_{pr}(\eta)=A_{pr}\exp(-2\ln 2\,\eta^2/\tau_{pr}^2)$, τ_{pr} and ω_{pr} are the duration [intensity full width at half maximum (FWHM)] and the carrier frequency, respectively, t_m is the time of the peak position of the input pulse with respect to one of the out-of-phase points $\eta=0$ (Fig. 1). From Eq. (33b) we obtain

$$s(z,\eta)=\frac{2}{\Omega}\arctan\left[\Gamma\tan\left(\frac{\Omega\eta}{2}\right)\right], \tag{35}$$

where the amplification parameter $\Gamma(z)=\exp[\gamma\Omega\int_0^z u_0(z')dz']$. This parameter increases exponentially with the Stokes shift Ω. On the other hand, for the impulsive regime the condition $\tau_{pu}<T_R$ has to be satisfied. Since u_0 increases with the pulse duration, a smaller value of Ω can be compensated by a larger duration of the pump pulse with the same intensity. $\Gamma(z)$ is determined by the change of the pump pulse during propagation, which significantly influences the amplitude-phase modulation for the probe pulse (see Sec. III B). Equations (33) take into account the decrease of the Raman amplitude $u_0(z)$ and generalize a solution given in Refs. [21,22] for constant u_0. The decrease of u_0 limits the maximum possible value of $\Gamma(z)$ for a given pump-pulse energy. This leads to one of the main limitations of shortest accessible durations by HSRS. The specific dependence of $u_0(z)$ on distance can be calculated numerically, as will be done in Sec. IV (see Fig. 12 below).

Here we estimate the optimum pump parameters and maximum possible $\Gamma(z)$. The Raman amplitude u_0 at $z=0$ for a Gaussian pump pulse can be found from Eq. (27) as

$$u_0=\frac{\sqrt{\pi}\alpha_{12}\tau_{pu}}{4\hbar\sqrt{\ln 2}}A_0^2\exp(-\Omega^2\tau_{pu}^2/16\ln 2), \tag{36}$$

where A_0 is the pump-pulse amplitude. Therefore, u_0 has a maximum for the pump-pulse input duration

$$\tau_{opt}=\sqrt{2\ln 2}\,T_R/\pi. \tag{37}$$

Due to the interaction with the medium the pump pulse is depleted and the amplitude of the Raman excitation is decreased. With the help of Eqs. (15), (27), and (37), the next-order approximation to Eq. (36) is found as follows:

$$u_0(z)=u_0(1-\sigma z), \tag{38}$$

where $\sigma=\sqrt{\pi}\gamma\alpha_{12}\Omega\tau_{pu}A_0^2/8\hbar\sqrt{\ln 2}$. This gives the amplification parameter

$$\Gamma(z)=\exp[\Omega\gamma u_0(z-\sigma z^2/2)], \tag{39}$$

which reaches the maximum possible value $\Gamma_{max}\approx 2$ independent of pump and medium parameters at distance $L_{opt}=1/\sigma$. However, L_{opt} depends on the pump energy and the medium. Here Γ_{max} is slightly underestimated because Eq. (39) is valid only for small distances.

The fluence which provides the maximum possible Raman amplitude $u_0=1$ and the population difference $w=0$ is

$$J_{max}\approx 1.6\frac{c\varepsilon_0\hbar}{\alpha_{12}}. \tag{40}$$

For typical Raman media $J_{max}\approx 4$ J/cm^2 which corresponds to a pump energy 0.6 mJ for a beam radius 70 μm and the typical Raman polarizability $\alpha_{12}\sim 10^{-41}$ Cm^2/V.

B. Amplitude-phase modulation and compression of a short probe pulse

In the method for the compression of single pulses by HSRS [21–23], the temporally delayed probe pulse with duration

$$\tau_{pr}<T_R \tag{41}$$

coherently interacts with the impulsively excited Raman medium. The analytical solution [Eqs. (34) and (35)] allows an understanding of the main physical features of the spectral broadening and phase-amplitude modulation of the probe pulse. In Figs. 2–5 this solution is presented for different parameters. But first, for better transparency we derive explicit expressions for the Fourier-transformed field $E_{pr}(\omega)$ in asymptotic approximation valid for the input probe pulse shorter than the period of the Raman oscillations [55].

The solution (34) is determined by the function $s(\eta)$ and the amplitude modulation factor $M(\eta)=\sin\Omega s/\sin\Omega\eta$. Both define the character of phase-amplitude modulation of the probe pulse by the Raman-active molecular modulator and are presented in Fig. 2(a). The function $s(\eta)$ (curve 1) oscillates periodically around the straight line $s=\eta$ and has the steepest slope at the out-of-phase points $t_o=lT_R$ ($l=0,\pm 1,\ldots$), where the main contribution to the phase modulation arises. In the vicinity of $\eta=t_o$, the expansion $s\approx t_o+\Gamma(\eta-t_o)-\Gamma\varepsilon(\eta-t_o)^3/3$ can be applied where $\varepsilon=(\Gamma^2-1)\Omega^2/4$. Near the in-phase points $t_i=(l+\frac{1}{2})T_R$, the function $s(\eta)$ has the smallest slope where $s\approx t_i+(\eta-t_i)/\Gamma+\varepsilon(\eta-t_i)^3/3\Gamma^3$. Then from Eq. (34) the main qualitative properties of the temporal pulse characteristics can be immediately seen, such as compression to a duration

$$\tau\approx\tau_{pr}/\Gamma, \tag{42}$$

a change of the instantaneous frequency spanning from

$$\omega_{min}\approx\omega_{pr}/\Gamma \tag{43}$$

to

$$\omega_{max}\approx\Gamma\omega_{pr}. \tag{44}$$

The instantaneous frequency near the peak of the probe pulse is

$$\omega(\eta)\approx\Gamma\omega_{pr}[1-\varepsilon(\eta-t_o-t_m)^2] \tag{45}$$

and has a linear and a quadratic chirp depending of the position of the input pulse t_m in respect of the out-of-phase points t_o of the Raman oscillations. At the out-of-phase point this chirp is purely quadratic. The peak amplitude and the pulse energy are increased by the factor Γ and the pulse peak

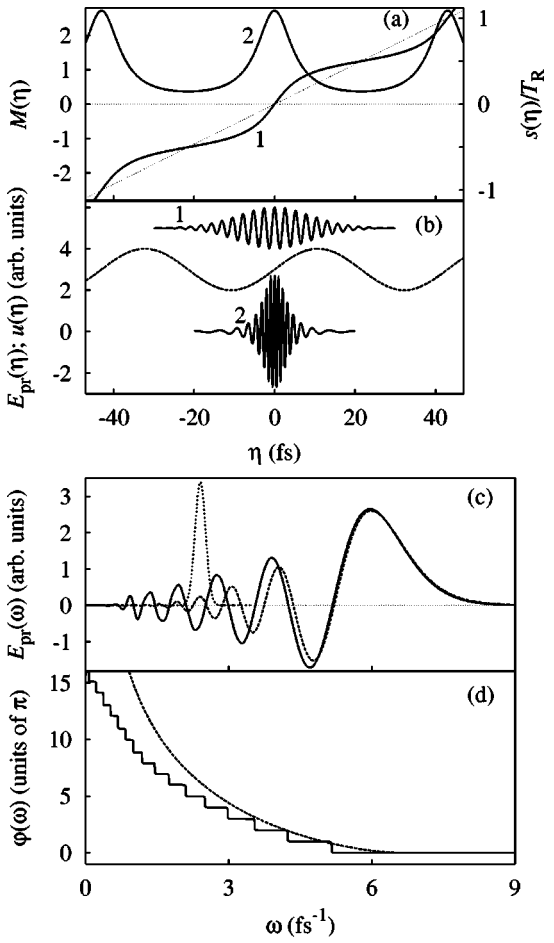

FIG. 2. Temporal and spectral characteristics of the solution, Eq. (34), for the out-of-phase position: (a) 1, function $s(\eta)$, 2, amplitude modulation factor $M(\eta)=\sin\Omega s/\sin\Omega\eta$; (b) 1, input probe pulse; 2, output pulse for $\Gamma=e^1$; dashed line, molecular oscillations; (c) solid line, spectrum of the probe pulse; dashed, approximation Eq. (50); dotted, input spectrum; (d) spectral phase of the output pulse; dashed, phase as defined by Eq. (49). The input pulse duration is 15 fs, wavelength is 790 nm, period of the molecular oscillation is 43 fs (SF_6).

is shifted towards the out-of-phase point $t_o=0$ as $t_m(z)\approx t_m/\Gamma$ due to the Raman-induced refractive index modulation.

By the change of the variables and using the relation $a(s)/a(\eta)=\partial s/\partial\eta$, the Fourier-transformed field can be presented in the form

$$E_{pr}(\omega)=\int_{-\infty}^{\infty}A_{pr}(s-t_m)\exp[i\omega_{pr}(s-t_m)-i\omega\eta]ds, \tag{46}$$

where $\eta=\eta(s)$ is the inverse function of Eq. (35). In the vicinity of the out-of-phase point, $\eta(s)$ can be approximated by $\eta\approx t_o+(s-t_o)/\Gamma+\varepsilon(s-t_o)^3/3\Gamma^3$. Then, to find the Fourier-transformed field (46) we use the stationary-point method and obtain

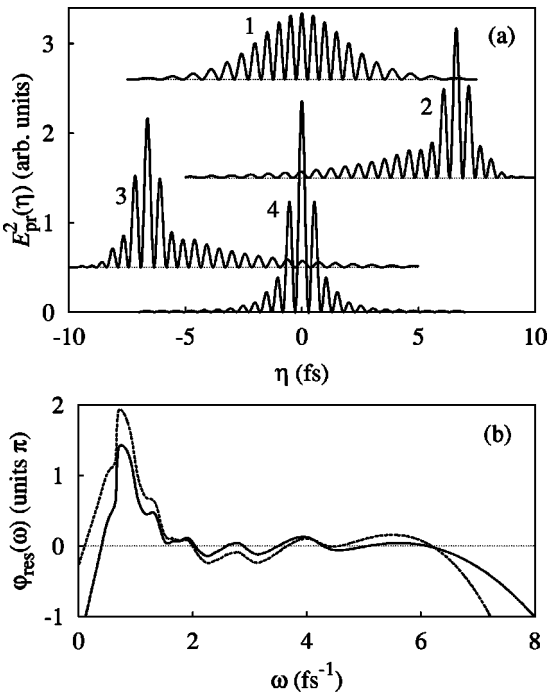

FIG. 3. Compression of the probe pulse in the out-of-phase position: (a) 1, probe pulse propagated in the Raman excited medium described by Eq. (34); 2, pulse after the phase compensation with $\varphi_c(\omega)=-0.9\omega^2$; 3, pulse after the phase compensation with $\varphi_c(\omega)=0.9\omega^2$; 4, pulse after ideal compression and (b) residual phase $\varphi_{res}(\omega)$ for $\varphi_c(\omega)=-0.9\omega^2$ (solid) and for phase compensation by a 18-μm-thick SiO_2 plate (dashed). All parameters are as in Fig. 2.

$$E_{pr}(\omega)=\frac{C}{\sqrt[3]{\varepsilon\omega}}[A_{pr}^{*}(s_0+t_m)\mathrm{Ai}(x)+A_{pr}(s_0-t_m)\mathrm{Ai}^{*}(x)], \tag{47}$$

where $\mathrm{Ai}(x)=\sqrt{\pi}\int_0^{\infty}\exp(ixs+is^3/3)ds$, $s_0^2=\Gamma^2(\Gamma\omega_{pr}-\omega)/\varepsilon\omega$, $x=(\omega-\Gamma\omega_{pr})/\sqrt[3]{\varepsilon\omega}$, and $C=\Gamma\exp(-i\omega t_m)/\sqrt{\pi}$. The expression (47) can be simplified by the asymptotics of $\mathrm{Ai}(x)$ [72]:

$$\mathrm{Ai}(x)=\begin{cases}\exp[-i\varphi_a(\omega)]/(-x)^{1/4} & \text{for } \omega<\Gamma\omega_{pr},\\ \exp(-2x^{3/2}/3)/2x^{1/4}+i\sqrt{\pi}/x & \text{for } \omega>\Gamma\omega_{pr},\end{cases} \tag{48}$$

where

$$\varphi_a(\omega)=\frac{2}{3}(\Gamma\omega_{pr}-\omega)^{3/2}/\sqrt{\varepsilon\omega}-\frac{\pi}{4}. \tag{49}$$

Let us now discuss the analytical solution (34) and the approximate expression (47) for different pump-probe delays. We consider the properties of the output probe for four characteristic delays when the peak of the input probe pulse has a position near (a) the out-of-phase point, (b) the minimum, (c) the in-phase point, and (d) the maximum with respect to the Raman oscillations (see Fig. 1).

(a) Out-of-phase delay $t_m=0$. In Fig. 2(b) the solution is presented for a 15-fs Gaussian input probe pulse (curve 1)

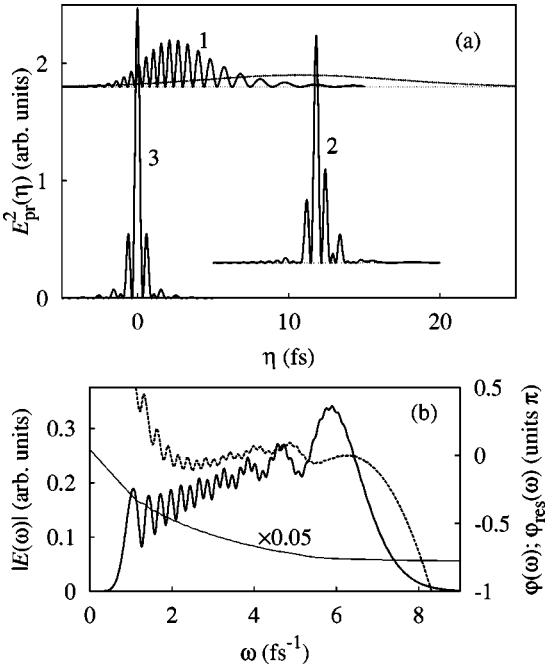

FIG. 4. Compression of the pulse in the position of the minimum: (a) 1, output probe pulse described by Eq. (34); 2, pulse after the phase compensation with $\varphi_c(\omega)=-0.9\omega^2$; 3, pulse after ideal compression; dotted line, input pulse envelope and (b) thick line, spectrum of the output pulse; thin, spectral phase; dashed, residual phase for $\varphi_c(\omega)=-0.9\omega^2$. All parameters are as in Fig. 2.

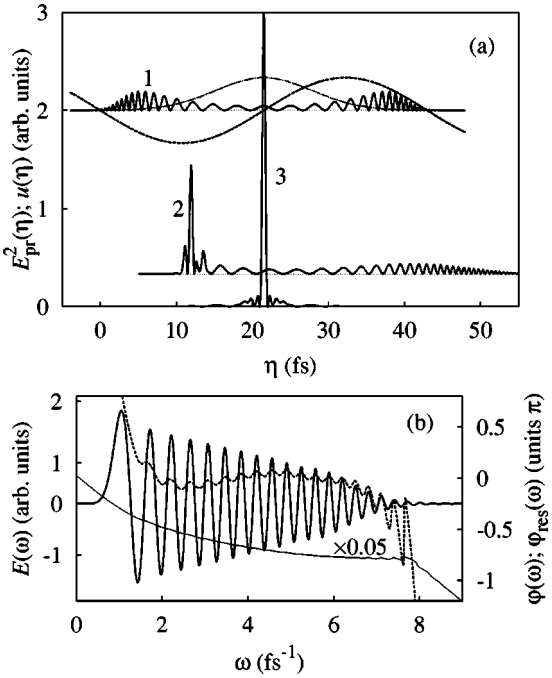

FIG. 5. The same as in Fig. 4 for an input probe pulse in the in-phase position.

together with the Raman oscillations $u(\eta)$ for $\Gamma=2.7$ and $T_R=43$ fs (SF_6). The output pulse (curve 2) is compressed to 4.4 fs, in agreement with the estimate (42). The pulse spectrum is significantly broadened and blue shifted with sign changes inside the spectrum. This specific behavior can be understood from the asymptotic expressions for $E_{pr}(\omega)$. For $t_m=0$ the field (47) is real and for $\omega<\Gamma\omega_{pr}$ can be written as

$$E_{pr}(\omega)=\frac{CA_{pr}(s_0)\cos\varphi_a(\omega)}{[\varepsilon\omega(\Gamma\omega_{pr}-\omega)]^{1/4}}. \tag{50}$$

Equation (50) rather precisely agrees with the numerically calculated value of the solution (34) [compare corresponding solid and dashed lines in Fig. 2(c)]. The spectral field $E_{pr}(\omega)$ changes its sign at frequencies where $\varphi_a(\omega)=(l+\frac{1}{2})\pi(l=0,1,\ldots)$ and the spectral phase presented in Fig. 2 (d) by solid line shows jumps to π. The dashed line in Fig. 2 (d) shows $\varphi_a(\omega)$ given by Eq. (49). The appearance of a jumplike phase modulation is rather unusual in ultrafast optics. At first glance, such jumps cannot be compensated by smooth dispersion to achieve pulse compression. However, as seen in Fig. 3, after phase compensation by normal group-velocity dispersion (GVD) characterized by the spectral phase $\varphi_c(\omega)=-\delta\omega^2$ with $\delta=0.9$ fs^2, the pulse is compressed to 1.3 fs (curve 2) and exhibits an asymmetric shape with a longer front. This unexpected behavior can be understood on the basis of Eq. (50) which can be expressed by two complex components with opposite spectral phases $\pm\varphi_a(\omega)$ and equal amplitudes. The compressor decomposes the pulse into two parts: a short bandwidth-limited pulse arising from the first component with the phase $\varphi_a(\omega)$ and a second long phase-modulated pulse arising from the second one with the phase $-\varphi_a(\omega)$. Pulse compression of the same pulse can also be achieved by a compressor with anomalous dispersion $\varphi_c(\omega)=\delta\omega^2$ and results also in a 1.3 fs pulse but with a longer edge at the front [Fig. 3 (a), curve 3]. From the representation of the cos function this rather surprising behavior can be easily understood.

From the bandwidth of the spectrum given by the minimum and the maximum frequencies (43) and (44) of the pulse, the shortest possible duration accessible after exact phase compensation can be estimated. Fitting of a shape-depending numerical factor in the relation $\tau_{min}\sim\Delta\omega^{-1}$ results in the pulse duration after ideal compression

$$\tau_{min}\approx 4\Gamma/\omega_{pr}(\Gamma^2-1). \tag{51}$$

An ideally compressed pulse is presented in Fig. 3 by curve 4. Equation (51) rather precisely predicts its duration of 1.1 fs. The important conclusion followed from Eq. (51) is that the ultimately shortest duration of the probe pulse is inversely proportional to ω_{pr} and Γ and independent of the input probe-pulse duration. However, the largest pulse duration for single-pulse compression is limited by the condition $\tau_{pr}<T_R$.

(b) Position in the minimum $t_m=T_R/4$. In Fig. 4 the solution [(34) and (35)] is presented for the same parameters as in Figs. 2 and 3 but with the delay in the minimum of the Raman oscillations. The output pulse compressed by propagation in the medium has the duration of 5.2 fs (curve 1), but shows a different phase modulation with a smooth spectral phase, as shown by the thin line in Fig. 4(b). The spectrum is

also significantly broadened (thick line) but in a more symmetric way. This different behavior can be understood on the basis of the asymptotic expression (47). For a delay in the range $T_R/20 \leq t_m \leq T_R/4$, the first term of Eq. (47) dominates. The spectral field can be approximated for $\omega < \Gamma\omega_{pr}$ as

$$E_{pr}(\omega) = \frac{CA_{pr}(s_0 - t_m)\exp[i\varphi_a(\omega)]}{[\varepsilon\omega(\Gamma\omega_{pr} - \omega)]^{1/4}}. \tag{52}$$

For $\omega > \Gamma\omega_{pr}$ the spectrum (47) decays exponentially and its phase $\varphi_a(\omega) = 0$. Now the field (52) has a smooth spectral phase (49) which does not depend on the pulse duration and can be compensated by normal dispersive elements with $\varphi_c(\omega) = -\delta\omega^2$ or by a piece of glass of fitted thickness. The spectral phase in Fig. 4(b) (thin line), of the exact solution (34), agrees well with Eq. (49). After compensation of this phase by normal GVD with parameter $\delta = 1.0$ fs^2, a shortened pulse [curve 2 in Fig. 4(a)] with a duration of 0.9 fs is obtained. For the duration of the ideally compressed pulse the same expression as Eq. (51) can be derived, which predicts well the duration in curve 3 in Fig. 4 (a). The difference to the out-of-phase point is mainly the fact that after the normal dispersive element the compressed pulse does not show a long tail, but the necessary phase of the compressor and the duration of the central output pulse are the same.

(c) In-phase delay $t_m = T_R/2$. In Fig. 5 (a) the solution (34) is presented by curve 1 for the in-phase delay. Now during propagation in the Raman medium the pulse is stretched and split into two parts with maxima arising near neighboring out-of-phase positions $\eta = 0$ and $\eta = T_R$, where the amplitude modulation function $M(\eta)$ in Eq. (34) is the largest and equals Γ. As seen from the carrier oscillations both parts have opposite chirps. The oscillating Fourier-transformed field presented in Fig. 5(b) is broadened in both red and blue sides but with higher amplitudes on the red side. The spectral phase of this pulse shows a smooth behavior. If the pulse passes through a piece of glass with normal dispersion, the first pulse with negative chirp is compressed into a subcycle pulse with duration 0.4 fs, while the duration of the second phase-modulated pulse is increased. An optical element with anomalous dispersion acts in opposite way; now the second pulse is compressed, while the first is prolonged. Note that for a delay near the in-phase position the asymptotic expression (47) is not valid.

(d) Position in the maximum $t_m = -T_R/4$. In this case the spectrum is the same as in Fig. 4, but the sign of the spectral phase is opposite. This pulse can be compressed by an optical element with anomalous dispersion. This fact is explained by the asymptotic expression (47). For a delay in the region $-T_R/4 \leq t_m \leq T_R/20$, the second term of Eq. (47) dominates and has a spectral phase $-\varphi_a(\omega)$. As will be shown in Sec. VI, this property can be used as a simple method for phase compensation in the MIR spectral region.

Let us summarize the results in this section for different delays. Near the minimum of the Raman oscillations the pulse has a smooth spectral phase given by Eq. (49), which can be compensated only by normal dispersion. Near the maximum the pulse has the smooth phase $-\varphi_a(\omega)$ which can be compensated only by anomalous dispersion. Near the out-of-phase point the spectral field is real and the phase shows jumps of π. Now a compressor with normal as well as anomalous dispersion with phases $\pm\varphi_a(\omega)$ decomposes the pulse into a short and a long part with the duration of the short part given by the Eq. (51). Near the in-phase point two pulses with the same amplitude and opposite sign of chirp are generated in the Raman medium. By an optical element with either normal or anomalous dispersion, one of the pulse is compressed while the other is suppressed.

C. Frequency-resolved pump-probe characterization

It is worth determining how the unusual features of phase-amplitude modulation given by Eq. (34) can be measured in real experiments. The full characterization of short frequency-modulated pulses is provided by heterodyne detecting of the instantaneous third-order nonlinear response in a frequency-resolved pump-probe (FRPP) geometry [73,74]. In FRPP the registered signal is described by

$$S(\omega,\tau) \propto \mathrm{Re}\left[E_{pr}^*(\omega)\int \left|E_{pr}(\eta+\tau)\right|^2 E_{pr}(\eta)\exp(i\omega\eta)\,d\eta\right], \tag{53}$$

arising from the interaction of two probe-pulse replicas, delayed by the time τ. The cross-correlation function (53), in dependence on frequency and delay allows one to reconstruct the amplitude and the phase of the pulse E_{pr}.

Figure 6 presents FRPP patterns of the initial pulse (a), the output probe pulse in the position of the out-of-phase point (b), and in the minimum (c) for $\Gamma = 2$ and other parameters as in Fig. 2. These traces reflect typical features corresponding to the character of the phase-amplitude modulation of the pulses presented in Figs. 2 and 4. In particular, for the out-of-phase input position the phase jumps of π take place just at the crests of positive and negative segments of the FRPP pattern in Fig. 6(b). Two branches of this pattern with opposite slopes correspond to the parts of the pulse for $\eta < 0$ and $\eta > 0$ with opposite frequency modulation. The main part of the FRPP pattern in the case of the input-pulse position in the minimum [Fig. 6(c)] has a slope which corresponds to a dominating contribution of the linear chirp [see Eq. (45)]. These FRPP patterns allow one to retrieve the features of the frequency modulation of the pulses by HSRS in real measurements.

D. Chirped input probe pulses

In some typical situations the experimentally available input probe pulses are not transform limited. As an example, the probe pulses in the visible, uv, or MIR generated by optical parametric amplification are usually phase modulated due to dispersion or SPM in the nonlinear crystal. The analytical solution [Eqs. (34) and (35)] is also valid for a general phase-modulated input probe pulse, where now for the input field the expression $E_{pr}(\eta) = A_{pr}(\eta)\cos[\omega_{pr}\eta + \phi(\eta)]$ has to be substituted with $\phi(\eta)$ describing the input phase modulation. In Fig. 7 the results are presented for an input phase modulation $\phi(t) = \frac{1}{2}\alpha\eta^2$ (where α is the chirp parameter)

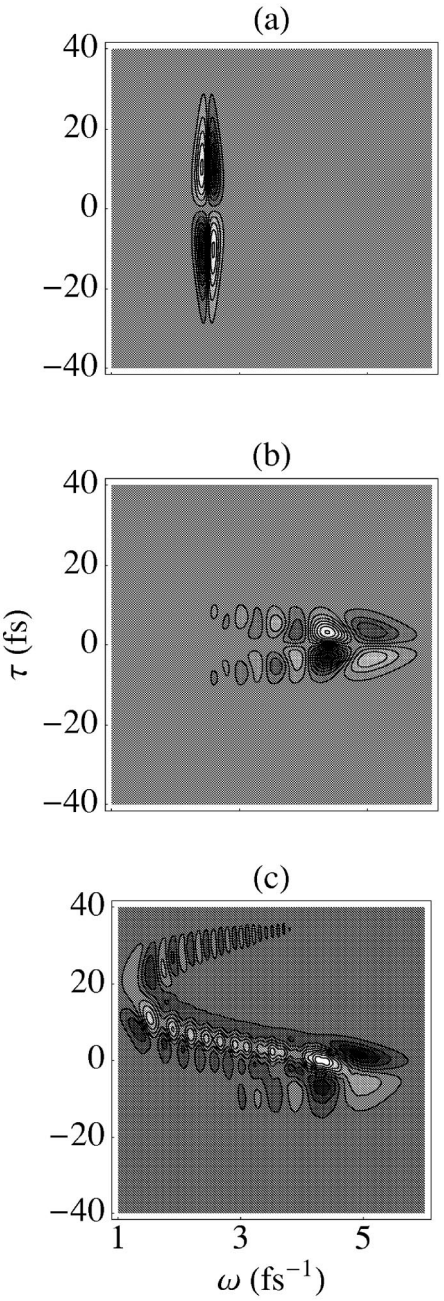

FIG. 6. Frequency-resolved pump-probe traces of the probe pulse Eq. (34) for (a) input, (b) out-of-phase position, and (c) minimum position, and for duration 15 fs, wavelength 790 μm, $\Gamma=2$, $T_R=43$ fs.

for an input pulse duration $\tau_{pr}=15$ fs at 790 nm and Raman parameters $\Gamma=e^1$ and $T_R=43$ fs in dependence on the chirp parameter α. The corresponding bandwidth-limited duration $\tau=\tau_{pr}/[1+(\alpha\tau_{pr}^2/8\ln 2)^2]^{1/2}$ characterizing the bandwidth of the chirped input pulse is presented by curve 1. Curve 2 shows the pulse duration after the propagation through the Raman medium and curve 3 the duration after the compression by ideal chirp compensation. The duration of the pulse after the Raman medium and after chirp compensation does not depend on the input chirp parameter α. This can be understood using the asymptotic approximation for $s(\eta)$.

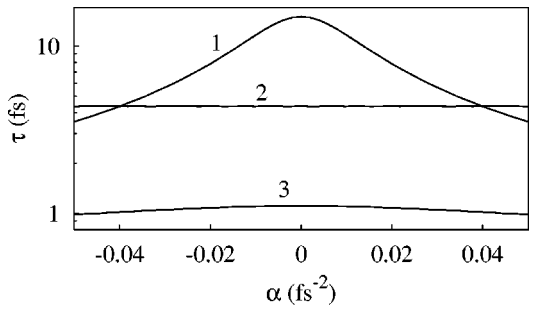

FIG. 7. Influence of the chirp on probe-pulse compression: corresponding bandwidth-limited duration of the chirped input pulse (curve 1), duration of the pulse after propagation in the Raman medium (curve 2), and duration of the ideally compressed output probe pulse (curve 3) versus chirp parameter. The parameters are as in Fig. 2.

Then the output chirp is given by $\omega(t)\approx\Gamma\omega_0[1-\varepsilon(t-t_m)^2]+\alpha\Gamma^2(t-t_m)$, where the contribution arising from the third term proportional to α is much smaller than the second one. This means that a chirp of the input probe pulse or a larger input bandwidth does not lead to a larger spectral broadening in comparison with an unchirped input pulse with the same duration. This result is consistent with the fact following from Eq. (51) that the ultimate duration of an unchirped probe pulse after compression does not depend on the input-pulse duration.

E. Phase-amplitude modulation of a long probe pulse

If the initial probe pulse is long in comparison with the period of Raman excitation T_R or a continuous wave (cw), the solution Eq. (34) takes the form

$$E_{pr}^{(cw)}(z,\eta)=A_{pr}\cos\Omega_{pr}s\frac{\sin\Omega s}{\sin\Omega\eta}, \tag{54}$$

where $s(z,\eta)$ is defined in Eq. (35). For simplicity we assume a rectangular shape for the input probe with pulse duration $\tau=(2M+1)T_R$ (M integer). In Fig. 8 (a) a certain time interval of the solution (54) for $M=25$ is shown by curve 1 together with the Raman oscillations (dashed line). During propagation through the Raman-excited medium the long input probe transforms into a train of compressed pulses located at out-of-phase points $t_o=lT_R$ with the repetition rate T_R and the envelope given by the factor $\sin\Omega s/\sin\Omega\eta$. The individual pulses have phase modulation described by the dependence $s(\eta)$.

The Fourier-transformed field of the train $E_{pr}^{(cw)}(\omega)=A_{pr}\int_{-\tau/2}^{\tau/2}\cos\Omega_{pr}s\exp(-i\omega\eta)ds$ can be found by the separation of the integration region to the segments $(l-\frac{1}{2})T_R<s<(l+\frac{1}{2})T_R$, whereby each segment belongs to an individual pulse in the train. Then one can obtain the spectrum as follows:

$$E_{pr}^{(cw)}(\omega)=E^{(1)}(\omega)\frac{\sin\left[\left(M+\frac{1}{2}\right)(\omega-\omega_{pr})T_R\right]}{\sin\left[\frac{1}{2}(\omega-\omega_{pr})T_R\right]}, \tag{55}$$

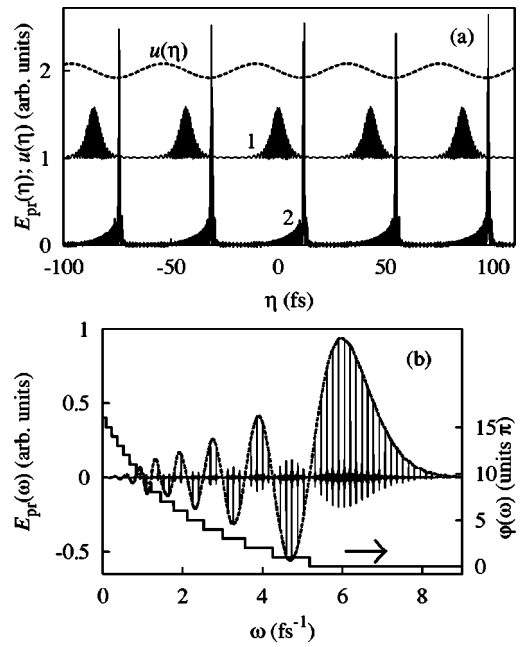

FIG. 8. Compression of a long probe pulse: (a) 1, temporal shape followed from Eq. (34); 2, compression by group-velocity dispersion with $\delta=0.9$ fs^2; dashed line, polarization of the medium and (b) spectral lines and spectral phase of the long probe pulse; dashed line, spectrum of a single pulse within the train (multiplied by the number of the pulses in the train). The parameters are as in Fig. 2.

where the spectrum of the individual pulses is given by $E^{(1)}(\omega)=A_{\rm pr}\int_{-T_R/2}^{T_R/2}\cos\Omega_{\rm pr}s\,\exp[-i\omega\eta(s)]ds$. In analogy with Sec. III B [see Eq. (50)], $E^{(1)}(\omega)$ can be approximated by

$$E^{(1)}(\omega)=\frac{CA_{\rm pr}\cos\varphi_a(\omega)}{[\varepsilon\omega(\Gamma\omega_{\rm pr}-\omega)]^{1/4}}. \tag{56}$$

If the input probe is a cw field, in the limit $M\to\infty$ the ratio in the right-hand side of Eq. (55) describes sharp spikes with amplitudes $2M+1$ at $\frac{1}{2}(\omega-\omega_{\rm pr})T_R=l\pi$, or at the spectral location of the Raman lines $\omega_l=\omega_{\rm pr}+l\Omega$. For finite M these spikes have a finite width $\sim 1/M$.

In Fig. 8(b) the spectrum of the long pulse is presented for $\Gamma=e^1$, demonstrating a large number of separated Raman lines with an envelope given by $E^{(1)}(\omega)$. The spectral field (55) is real, but shows sign changes. An important conclusion followed from Eq. (55) is that the envelope of the multiple separated Raman lines and the spectral phases with jumps from 0 to π within the spectrum follow the same behavior as for a short input pulse with $\tau_{\rm pr}<T_R$ [compare with Fig. 2 and Eq. (50)]. This means that the envelope of the spectral lines and the spectral phase modulation is determined by the individual pulses formed during propagation within the train. The latter is only weakly depending on the duration of the initial long probe pulse.

Therefore, similar to the case of a short input pulse with $\tau_{\rm pr}<T_R$ and a delay $t_{\rm m}=t_{\rm o}$, the individual pulses in the train can be compressed by optical elements with normal or anomalous dispersion. The compression of each individual pulse in the train is shown in Fig. 8 (a) (curve 2) for a chirp compensator with $\delta=-0.9$ fs^2. As can be seen, the compressor decomposes each individual pulse into a short bandwidth-limited and a long phase modulated part, in analogy with Fig. 3 for a short input at out-of-phase initial position. The ultimate shortest duration of the individual pulses is also given by the same relation (51) as for short input pulses. Note that for the case of small Raman excitation $\ln\Gamma\ll 1$ and $\tau_{\rm pr}\gg T_R$, the compression of the pulses in the train by external group-velocity dispersion was discussed in Ref. [17] for the adiabatic regime and measured in Refs. [19,23] for the pump-probe regime.

F. Phase mismatch and walk-off effects due to dispersion

If pump and probe pulses have different input frequencies, the difference in the phase and group velocities of both pulses due to dispersion results in phase mismatch and probe-pulse walk off in respect of the Raman excitation and their interaction becomes less effective. This effect can be described approximately with the neglect of the difference between phase and group velocities and the decrease of the Raman amplitude u_0 during propagation, taking into account only the difference of the input-pulse velocities. Using a shift of the moving time $\eta\to\eta-n_{\rm pu}z/c$, the evolution equation (15) for the probe pulse takes the following form:

$$\left(\frac{\partial}{\partial z}-\Delta\frac{\partial}{\partial\eta}\right)E_{\rm pr}=-\frac{\mu_0 c}{2}\frac{\partial P_R}{\partial\eta}, \tag{57}$$

with $\Delta=[n(\omega_{\rm pu})-n(\omega_{\rm pr})]/c$. Comparing with Eq. (28) we see that the general solution Eq. (33) can be used also for this situation with $a(\eta)=u_0\sin\Omega\eta-\kappa$, where $\kappa=\Delta/\gamma u_0$. Substituting the latter into Eq. (33b) we find the relation implicitly defining $s(z,\eta)$:

$$\ln\frac{\kappa\tan(\Omega s/2)+\sqrt{1-\kappa^2}-1}{\kappa\tan(\Omega s/2)-\sqrt{1-\kappa^2}-1}$$
$$=\ln\tilde{\Gamma}\frac{\kappa\tan(\Omega\eta/2)+\sqrt{1-\kappa^2}-1}{\kappa\tan(\Omega\eta/2)-\sqrt{1-\kappa^2}-1}, \tag{58}$$

where $\tilde{\Gamma}(z)=\exp[\Omega\gamma u_0\sqrt{1-\kappa^2}z]$ while the output probe field is given by

$$E_{\rm pr}(z,\eta)=E_{\rm pr}(s)\frac{\sin\Omega s-\kappa}{\sin\Omega\eta-\kappa}. \tag{59}$$

For $\kappa>1$ the connection between the logarithmic function with complex argument with the trigonometric functions has to be used.

It is interesting that the solution [Eqs. (58) and (59)] depend on the linear dispersion parameter Δ only through the ratio κ which expresses a combined influence of the refractive index change both by linear dispersion and the Raman effect. As discussed in Sec. III B, the Raman effect leads to a shift of the pulse maximum towards the out-of-phase position and therefore walk off is influenced not only by linear

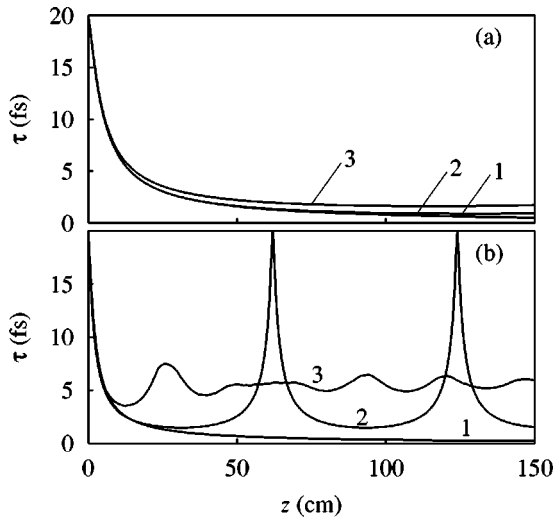

FIG. 9. Influence of phase mismatch and walk off: the duration of the probe pulse after exact phase compensation is presented versus distance for a probe pulse wavelength 395 nm (a) and 158 nm (b) in a hollow waveguide with radius $R=70$ μm filled by SF_6 at 0.3 atm. Curve 1 is obtained from Eqs. (34) and (35), curve 2 from Eqs. (58) and (59), and curve 3 from the numerical solution of Eqs. (15) and (17). The pump pulse at 790 nm has the duration 20 fs and intensity of 50 TW/cm^2 and the input probe-pulse duration is 20 fs.

dispersion but also by the Raman parameters, which explains the specific dependence of the solution [Eqs. (58) and (59)] on κ.

To analyze the solution [Eqs. (58) and (59)], in Fig. 9, for a waveguide filled with SF_6, we have presented by curve 2 the probe-pulse duration after exact phase compensation in dependence on the waveguide length for a pump at 790 nm and a probe at 395 nm (a) and 158 nm (b). The probe-pulse duration after ideal compression characterizes the spectral width due to spectral broadening by the Raman modulation, i.e., the shortest accessible duration by this method, and is calculated from the FWHM of the field $E_c(\eta) = \int_{-\infty}^{\infty} \exp(i\omega\eta)|E_{\mathrm{pr}}(\omega)|d\omega$, where $E_{\mathrm{pr}}(\omega)$ is the Fourier-transformed field obtained from Eq. (59). For a comparison, we also present the probe-pulse duration after exact phase compensation with the neglect of the linear dispersion described by the solution Eqs. (34) and (35) (curves 1) and the pulse duration obtained from the numerical solution of the full model described by Eqs. (15)–(17), which takes into account the full influence of dispersion and pump-pulse changes during propagation (curves 3). More details of the numerical simulations are presented in Sec. IV. The intensity of the 20-fs pump pulse is 50 TW/cm^2 and for the chosen waveguide and medium dispersion parameters we have found numerically that the excitation amplitude $u_0(z=0) \approx 0.2$ and the characteristic parameter $\kappa \approx -4$ and -15 for curves 2 in Figs. 9(a) and 9(b), respectively.

The curves 1 and 2 in Fig. 9(a) are almost identical and show only a very small deviation from the result of the exact model presented by curve 3. For the considered parameters in the optical range, the influence of the dispersion is obviously weak and the solution [Eqs. (58) and (59)] does not give a better description compared with Eqs. (34) and (35), but both give an excellent description of the probe-pulse phase-amplitude modulation. For a vuv probe at 158 nm the solution [Eqs. (58) and (59)] presented by curve 2 give the same duration as the solution [Eqs. (34) and (35)] for a small propagation length, but a large difference to curve 1 and a periodic behavior for longer propagation, which is typical for nonphasematched nonlinear interaction processes. However, curve 3 obtained by the exact numerical solution also significantly differs from curve 2. Obviously, in the uv-vuv spectral region the difference in phase and group velocities, the spectral changes during propagation, the decreasing Raman amplitude $u_0(z)$ with propagation, and second and high-order dispersion effects play a significant role in the ultrawide spectral broadening process for longer propagation lengths. These effects have to be studied numerically, as will be done below in Secs. IV–VI. On the other hand, the smallest pulse duration after ideal compression or the largest bandwidth in curve 3 of Fig. 9(b) is achieved already after propagation of about 10 cm. At this distance the curves 1 and 2 completely agree and show no significant deviation from curve 3. Note that this distance has to be chosen in real compression experiments, because at longer propagation length the pulse is split into subpulses with different signs of the chirp, which cannot be compensated by normal dispersive elements. This means that for optimum propagation lengths the simpler solution, from Eqs. (34) and (35) instead of Eqs. (58) and (59), can also be used in the uv-vuv region for a realistic description of the main physical properties of the probe pulse, but a full numerical simulation is necessary in order to find these optimum conditions with a reduced influence of dispersion using pressure optimization.

G. Comparison with the slowly varying envelope approximation for small Raman conversion

Let us derive from Eqs. (34) and (35) approximate expressions for a probe pulse in the Raman-excited medium in the case of a small conversion efficiency $\ln\Gamma \ll 1$, and compare the above results with corresponding expressions with the use of SVEA. For this limiting case, from Eq. (35) we find $s \approx \eta + \tilde{\Gamma}\sin\Omega\eta$, where $\tilde{\Gamma}(z) = \gamma\int_0^z u_0(z)\mathrm{d}z$, and obtain

$$E_{\mathrm{pr}}(z,\eta) = A_{\mathrm{pr}}(\eta - t_{\mathrm{m}})\cos\Omega_{\mathrm{pr}}(\eta - t_{\mathrm{m}} + \tilde{\Gamma}\sin\Omega\eta). \quad (60)$$

This is a frequency-modulated pulse without temporal amplitude modulation and this means that it does not become shorter during propagation. With the use of the relation $\exp(ix\sin\Omega\eta) = \Sigma_l J_l(x)\exp(il\Omega\eta)$ [72], the Fourier-transformed field is given by

$$E_{\mathrm{pr}}(\omega) = \sum_{l=-\infty}^{\infty} J_l A_{\mathrm{pr}}(\omega_{\mathrm{pr}} + l\Omega - \omega)\exp[i(l\Omega - \omega)t_{\mathrm{m}}], \quad (61)$$

where $J_l = J_l(\tilde{\Gamma}\omega_{\mathrm{pr}})$ are the Bessel functions and $A_{\mathrm{pr}}(\omega)$ is the Fourier-transformed pulse envelope. If the input pulse is long with duration $\tau_{\mathrm{pr}} \gg T_{\mathrm{R}}$, the different terms in Eq. (61) describe discrete high-order Raman components which are symmetric in respect of the input carrier frequency (it is sup-

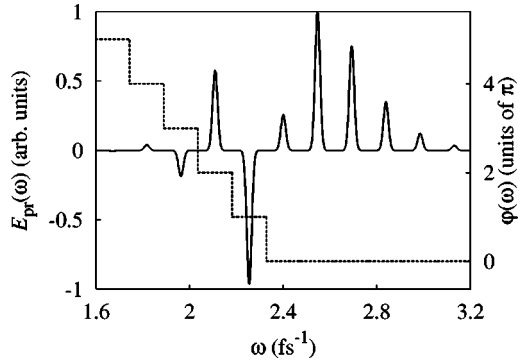

FIG. 10. Spectrum (solid line) and spectral phase (dashed) of a long probe pulse for small Raman excitation. Duration is 150 fs, $\Gamma=1.14$, and other parameters are as in Fig. 2.

posed that $\tilde{\Gamma}\omega_{pr}<2.405$). Independent from the delay t_m the components have the same phase in anti-Stokes side and change their sign periodically with l on the Stokes side, owing to $J_{-l}=(-1)^l J_l$ [Fig. 10 (a)]. Therefore, at the Stokes side the spectral phase jumps between 0 to π (dashed line).

For a short probe pulse with $\tau_{pr}<T_R$, the Raman components given by Eq. (61) are broadened and merged into a continuous spectrum with a shape which is defined by their amplitudes and the phases. If the probe pulse is in the out-of-phase point, only the Stokes components show sign changes and therefore, due to destructive interference the spectrum is shifted to the anti-Stokes side analogous as in Fig. 2 for a large Raman conversion. If the probe pulse is in phase with molecular oscillations, only the spectral components on the anti-Stokes side change the sign and the spectral phases jump from 0 to π. Therefore, the spectrum is shifted to the Stokes side (compare Fig. 5). However, as shown above, with increasing $\tilde{\Gamma}$ these simple relations between the Raman components and their phases are violated and the solution Eqs. (34) and (35) should be used instead of Eqs. (60) and (61) to characterize ultrawide spectral broadening by HSRS.

An analogous Bessel-like distribution of the spectrum can be obtained for the regime of two-color excitation when two cw input-pump fields with frequencies ω_{pu} and $\omega_S=\omega_{pu}-\Omega$ with amplitudes A_0 and A_S, respectively, excite the medium and are influenced by the interaction with Raman oscillations and produce a comb of Raman lines. For this regime, in analogy with Eq. (60), we find from Eqs. (34) and (35) the field

$$E(z,\eta)=A_0\cos\Omega_{pu}[\eta+\tilde{\Gamma}\sin(\Omega\eta+\psi)] + A_S\cos\Omega_S[\eta+\tilde{\Gamma}\sin(\Omega\eta+\psi)], \quad (62)$$

where ψ is the phase resulted from Eq. (27) for $a_2\neq 0$. Analogous to Eq. (61), the Fourier-transformed field (62) presents a comb of Raman lines located at frequencies $\omega_l=\omega_{pu}+l\Omega$. In the spectral representation it can be written as $E(z,\eta)=\Sigma_l E_l(z)\exp(i\omega_l\eta)$ with

$$E_l(z)=A_0 J_l(\tilde{\Gamma}\omega_{pu})\exp(il\psi)+A_S J_{l+1}(\tilde{\Gamma}\omega_S)\exp[i(l+1)\psi]. \quad (63)$$

The phase relations between different spectral components depend on the phase ψ and show a similar behavior as shown in Fig. 10 for the special value $\psi=0$.

Results analogous to Eqs. (62) and (63) have been derived earlier in Refs. [17,43], starting from the basic Eq. (18) using the SVEA and neglecting phase mismatch $\Delta_l=0$. The Bessel-like distribution of the spectral intensity followed from Eq. (61) for the case of a pump-probe regime with short input pump and long probe pulses was studied in Ref. [53]. However, it should be noted that the phases of the different Raman lines are not locked as assumed in this paper but shows, as shown above, jumps of π. Obviously, the case of two-color excitation described by Eqs. (62) and (63) as well as the case of the pump-probe regime described by Eqs. (60) and (61) leads to analogous formulas. These results are obtained with the use of SVEA and are consistent only if the condition (2a) or $\ln\Gamma\ll 1$ is fulfilled, i.e., for small spectral broadening. However, for ultrabroadband spectral broadening a large modulation factor $\ln\Gamma>0.5$ is required, therefore a theoretical analysis without the use of SVEA is necessary, as done in Refs. [21,22] and discussed in detail in the preceding sections.

IV. COMPRESSION OF VISIBLE PULSES: NUMERICAL RESULTS

A. Impulsive excitation by single pump pulses

In order to find analytical solutions in most parts of Sec. III, the influence of linear dispersion was neglected. In Section III F dispersion was discussed by taking into account the different velocities of the input pulses but neglecting the change of the pump pulse and the decrease of the Raman amplitude during propagation. We have seen that dispersion does not play a significant role in the optical range for certain optimized parameters. However, whether dispersion plays a major role or can be neglected sensitively depends on the chosen spectral range and other parameters. In general, velocity walk off causes physical limitations of the shortest pulse durations due to the shift of the position of pulse maximum to the in-phase point, which typically leads to a pulse splitting after a certain propagation length. Besides, dispersion is the reason for an additional contribution to the spectral phases. Normal GVD of the gas filling leads to the compression of the pulse during propagation if the delay is in the range $T_R/20\lesssim t_m<T_R/2$ in the same way as the glass window acts beyond the waveguide. The unfavorable influence of the walk-off effect can be reduced by dispersion control using the contribution of the waveguide to dispersion given by Eq. (16) and optimizing the pressure. In Fig. 11 the group delay and the GVD parameter in dependence on the frequency is presented for a waveguide with different gas pressure and radius. For SF_6 pressure 1 atm and waveguide radius 70 μm, the delay time between a pump pulse at 800 nm and a probe pulse at 400 nm is $\sim$100 fs after 1 m, but this value can be reduced to $\sim$15 fs for a lower pressure 0.3 atm. The GVD parameter at 0.3 atm is significantly smaller than for 1 atm in

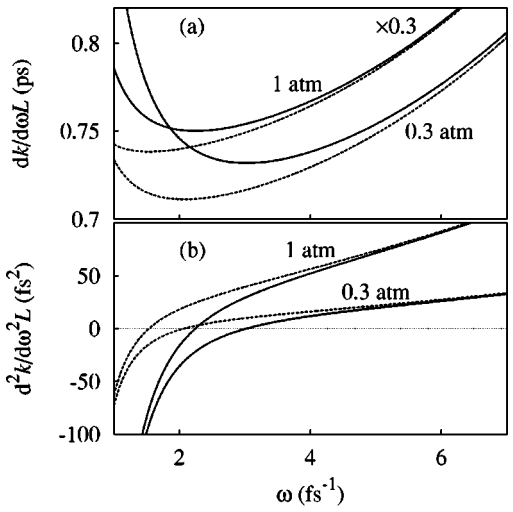

FIG. 11. Group delay (a) and group-velocity dispersion (b) vs frequency in a hollow waveguide filled by SF_6 for distance $L=1$ m, waveguide radius 70 (solid lines) and 150 μm (dashed), and gas pressure as indicated.

the whole optical domain and is anomalous for the pump and normal for the probe. On the other hand, a lower pressure leads to a smaller modulation parameter Γ and therefore the optimum pressure can only be found numerically, using the solution of the propagation problem with different pressures and radii. In addition to dispersion of the linear refraction, the Raman-induced refractive index change influences the position of the probe pulse and leads to a shift toward the out-of-phase position. Note that dispersion control in waveguides has been used previously for four-wave mixing in Ref. [75] and was theoretically studied for SPM-induced pulse compression in Ref. [61] and for multiple Raman line generation in Ref. [54].

To analyze the full influence of dispersion with phase mismatch, walk off, GVD as well as higher-order dispersion effects, and the change of the pump pulse we have solved numerically the full basic equations given in Eqs. (15)–(17). We study pulse propagation in a waveguide filled with SF_6 with $\alpha_{12}=1.3\times10^{-41}$ Cm^2/V, $C_1=0.7$ fs^{-2}, and $\omega_1=31.9$ fs^{-1} [76,77].

The Raman amplitude and the pump-pulse change with propagation (Figs. 12 and 13, respectively). The Raman amplitude decreases more strongly for a higher input-pump intensity (curve 2) while the change is smaller for a lower intensity (curve 1). The decrease of u_0 is explained by the change of the pump pulse [compare Figs. 13(a),(b)], because part of the pulse energy is stored in the medium and therefore the energy of the pump pulse is reduced during propagation. In addition, as presented in Fig. 13(c) the spectrum of the pulse is shifted to smaller frequencies, since the Raman modulation created by the pump pulse itself arises mainly at the in-phase position [see Eq. (27)].

In Fig. 14 the shape and the spectrum of a 20-fs, 395-nm input probe pulse is presented after propagation through SF_6 for a distance 1 m, a pressure 0.3 atm, a waveguide radius 70 μm, and for four characteristic positions to the input probe pulse in respect of the Raman oscillations. The temporal shapes are presented in the left and the spectra in the right sections. For a probe-pulse position in the minimum of Raman oscillations with delay $t_m=T_R/4$, the spectrum is almost symmetrical and has the width $\Delta\omega\approx3.5$ fs^{-1} [Figs. 14(a),(b)]. It shows a behavior analogous to that described by the analytical formula in Eq. (52) with a quasioscillating behavior. In difference to the analytical results, now the spectral phase is compensated by normal dispersion of the medium itself and the changes of the output-pulse phase is much smaller than π in a rather large spectral interval [Fig. 14(b), dashed curves]. Therefore, an extremely short pulse with duration of 1.7 fs is formed during propagation in the Raman medium itself, close to the bandwidth-limited value. For the out-of-phase delay $t_m=0$ [Figs. 14(c),(d)], the maxi-

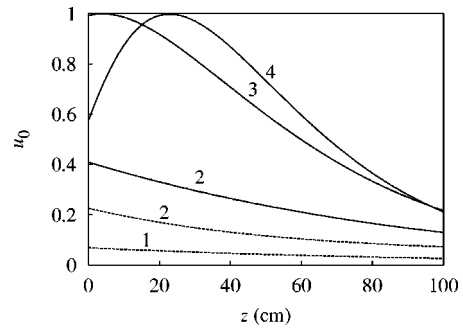

FIG. 12. Amplitude of the Raman excitation for a pump intensity $I_0=15$ TW/cm^2 (1), 50 TW/cm^2 (2), and for a sequence of 10 (3) and 15 (4) pulses with the intensity 20 TW/cm^2 in SF_6 (dashed curve) and molecular *para*-H_2 (solid) at pressure 0.3 atm and length 1 m. Initial pump-pulse duration $\tau_{pu}=20$ fs, wavelength $\lambda_{pu}=790$ nm, and hollow waveguide radius $R=70$ μm.

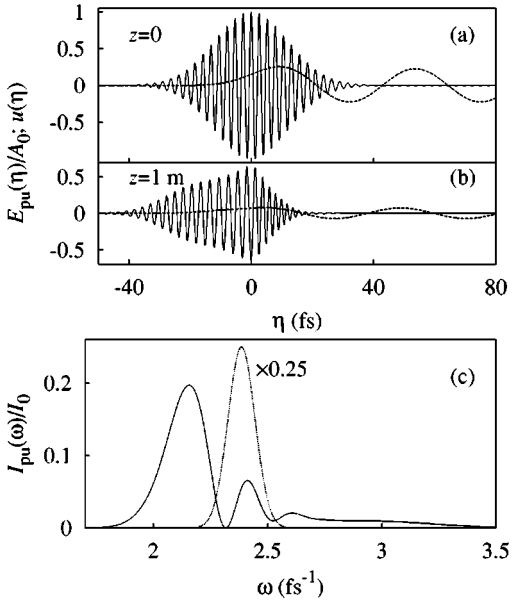

FIG. 13. Change of the pump pulse in the hollow waveguide filled with SF_6 gas: (a) initial pump pulse (solid line) and medium polarization (dashed); (b) pump pulse (solid) and medium polarization (dashed) at $z=1$ m; and (c) initial (dotted) and output (solid) spectrum. The initial pump-pulse intensity is $I_0=50$ TW/cm^2 and other parameters are as in Fig. 12.

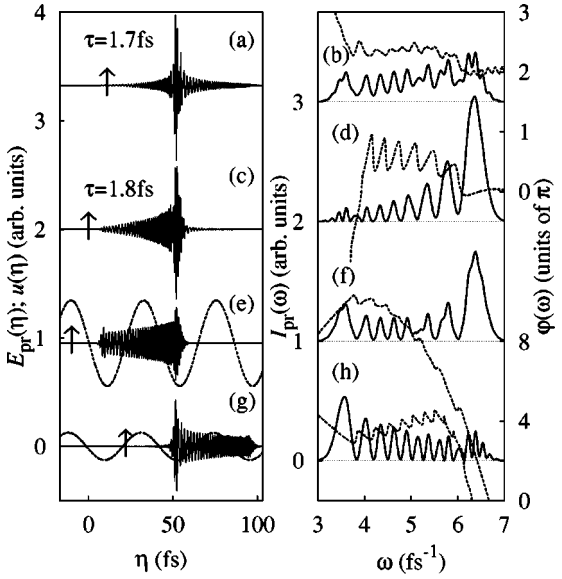

FIG. 14. Numerically calculated temporal shapes (left column) and spectral characteristics (right) for a 20-fs input probe pulse at 395 μm in a hollow waveguide filled with SF_6. The spectra and spectral phases are plotted by solid and dashed lines, respectively. The input position shown by arrows is in the minimum (a),(b), the out-of-phase point (c),(d), the maximum (e),(f), and the in-phase point (g),(h). Dashed lines present the Raman oscillations at the waveguide input (e) and the output (g). The pump intensity is 50 TW/cm^2 and other parameters are as in Fig. 12.

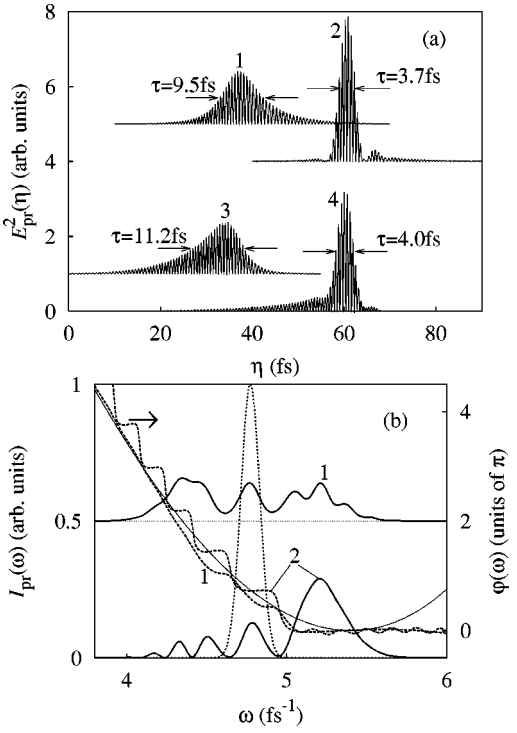

FIG. 15. Temporal (a) and spectral (b) characteristics for comparison with the experimental measurements reported in Ref. [23]. The upper parts refer to the minimum and the lower parts to the out-of-phase position of the input probe. In (a) the pulse shapes after propagation (curves 1,3) and after compression by 86-μm SiO_2 plate (2,4) are presented. In (b) spectra (solid lines) and spectral phases (dashed), initial probe spectrum (dotted), and glass plate phase with the opposite sign (thin) are shown. The intensity of the pump pulse is 15 TW/cm^2 and other input pump and probe parameters are as in Fig. 14.

mum of the spectrum is significantly enhanced on the blue side and the spectrum shows zeros located near the positions predicted by Eq. (50). In this case the temporal shape shows a short bandwidth-limited pulse with duration of 1.8 fs and a long phase-modulated part. This agrees with the scenario of pulse compression near the out-of-phase position as described in Sec. III B. The Raman medium now acts as phase modulator, which broadens the spectrum and causes phase jumps of π within the spectrum, and as compressor with normal GVD, which decomposes the pulse into a bandwidth-limited short and a phase-modulated long part. For an initial probe delay at the maximum of Raman oscillations, we find the opposite behavior [Figs. 14(e),(f)] compared with the position in the minimum, as the chirps, both due to the medium dispersion and the Raman modulation, have the same sign. This explains the temporal shape in Fig. 14(e) with a long front. For the case of the in-phase delay $t_m = T_R/2$ presented in Figs. 14(g),(h), the Raman amplitude modulation splits the pulse into two parts with approximately the same peaks and located at neighboring out-of-phase points. However, the additional normal GVD of the medium compresses the front part of the pulse and leads to a suppression of the tail maximum as seen in Fig. 14(g). This is analogous to what was found by the analytical solution in Fig. 5 and is explained by the negative sign of the frequency chirp in the time range $T_R/20 \lesssim \eta < T_R/2$ (when blue frequencies precede red) and the positive sign for $-T_R/2 < \eta \lesssim T_R/20$.

The results in Fig. 14 are obtained for a rather high intensity, but still below the ionization threshold. With decreasing pump-pulse intensity the probe spectrum is narrower and the duration longer. As an example, in Fig. 15 the results are presented for a 20-fs pump pulse at 790 nm with an intensity of 15 TW/cm^2. For two different locations at minimum of the Raman oscillations [upper sections in Fig. 15(a,b)] and at the out-of-phase point (lower sections), a 20-fs input probe pulse at 395 nm is broadened to a width of 1.2 fs^{-1}. The spectral phases presented by the dotted line in Fig. 15(b) demonstrate that the pulse is still significantly phase modulated. Therefore, after propagation the duration of 9.5 or 11.2 fs is longer than the corresponding bandwidth-limited value. However, normal GVD of a 82-μm fused silica plate compresses this pulse to a duration of 3.7 fs or 4.0 fs at the minimum and out-of phase position, respectively. The parameters chosen in Fig. 15 are the same as in the experiment in Ref. [23] , if an effective reduction factor is taken into account due to the transverse-mode distribution in the waveguide. The predicted pulse duration and the spectral width are in good agreement with the measured duration 3.8 fs and the spectrum between 350 and 460 nm.

In order to justify the above given interpretation concerning the influence of dispersion, in Fig. 16 we compare the results of two simulations with (curves 1) and without (curves 2) dispersion for the probe pulse. The temporal shape of the pump pulse is more strongly influenced by the addi-

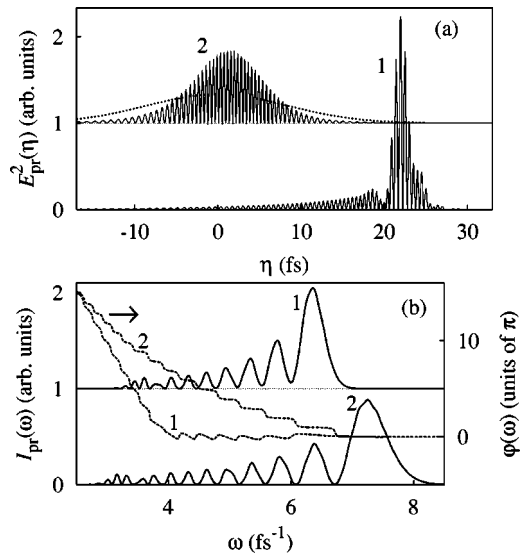

FIG. 16. Influence of the medium and hollow fiber dispersion on the temporal (a) and spectral (b) characteristics of the probe pulse: 1, with material and waveguide dispersion; 2, without. Dotted lines show the envelopes and spectra of the input probe pulse. The duration of the probe pulse at distance 1 m is 1.8 (1) and 9.7 fs (2). The intensity of the pump pulse is 50 TW/cm^2 and other parameters are as in Fig. 14.

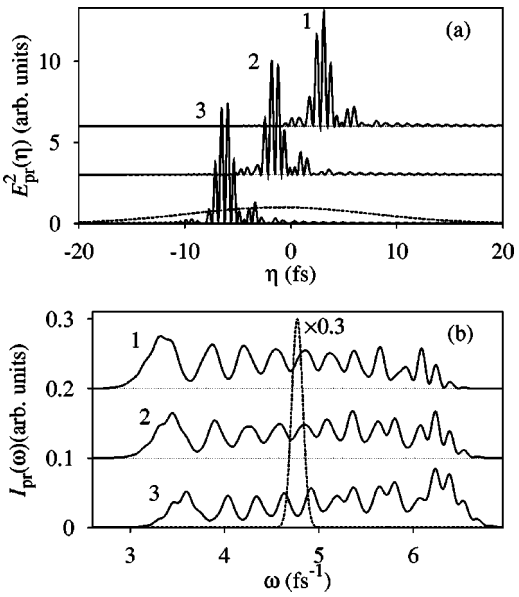

FIG. 17. Influence of the SF_6 pressure on temporal (a) and spectral (b) characteristics of the probe pulse for the same pressure-length product: 1, pressure 1 atm, distance 0.3 m, 2, 0.5 atm, 60 cm, 3, 0.3 atm, 100 cm. All input pump and probe pulse parameters are as in Fig. 14. In all three cases the output duration is the output probe pulse is 1.7 fs.

tion of dispersion, while the spectral changes with redshifted maxima are similar in both cases. With inclusion of dispersion the spectrum of the probe pulse shown in Fig. 16(b) is somewhat narrower, while the pulse duration of 1.8 fs is significantly smaller than in the case without dispersion, which yields a 9.7-fs pulse after the Raman medium. The spectral phases shown by dashed lines in Fig. 16(b) explain this large difference in the temporal behavior. Without dispersion the spectral phase shows the jumplike behavior typical for the out-of-phase delay as described by Eq. (50). With inclusion of dispersion of the Raman medium, the change of the spectral phase of the output probe pulse [Fig. 16 (b), curve 1] is much smaller than π almost in the whole spectrum. This explains the decomposition of the pulse into a short central part and a long wing for the out-of-phase initial position and demonstrates the simultaneous action of phase modulation by HSRS and phase compensation due to linear dispersion of the gas filling.

From the results presented in Figs. 14 –16 the conclusion can be drawn that in the optical range the effects of phase mismatch and walk-off effect are relatively weak and dispersion introduces mainly an additional spectral phase which can be used for compensation of the Raman-induced spectral phase. This fact is supported by Fig. 17, where the temporal shapes and spectra of the output probe pulses are presented for different pressures but the same product of pressure and length of the waveguide. For the input probe position we use the minimum of the Raman excitation. As seen, the spectrum and pulse duration of the probe pulses do not change significantly for different pressures but with the same pressure-length product.

The above described weak influence of the walk-off effect in the optical frequency domain allows an approximate rescaling of the optimum parameters. If dispersion is not taken into account, the propagation problem in the Raman-excited medium depends mainly on dimensionless parameters $\mu_0 c \alpha_{12} NL/\tau_{pr}$ and $\alpha_{12} A_0^2 \tau_{pu}/\hbar$, $\Omega \tau_{pu}$ and $\Omega \tau_{pr}$. Therefore, for optimum conditions a smaller propagation length L requires a correspondingly higher pressure. However, this relation is not valid in general. In particular, for probe pulses in the uv-vuv spectral region, the influence of dispersion becomes stronger and has to be considered carefully, as shown in Sec. V.

B. Impulsive excitation by pulse sequences

In order to generate still shorter pulses, a larger modulation factor Γ has to be realized over a short propagation distance before walk off and higher-order dispersion effects cause pulse splitting during propagation in the Raman-excited medium. By increasing the pump intensity the amplification parameter Γ can be increased, but the highest intensity is limited by the ionization threshold. A possible method to increase Γ but avoid ionization is the excitation of the Raman medium by a pulse sequence synchronized to the Raman period and with intensities of the individual pulses below the ionization threshold [40]. With the well-developed technique for shaping of ultrashort pulses by spatial light modulators, the generation of pulse sequences is a feasible experimental method.

The Raman amplitude $u_0(z=0)$ for pumping by a sequence of $M+1$ pulses with the field strength

$$E_{pu}(\eta) = A_0 \sum_{l=0}^{M} \exp\left[-2 \ln 2 \left(\frac{\eta - l T_S}{\tau_{pu}} \right)^2 \right] \cos \omega_{pu} \eta, \tag{64}$$

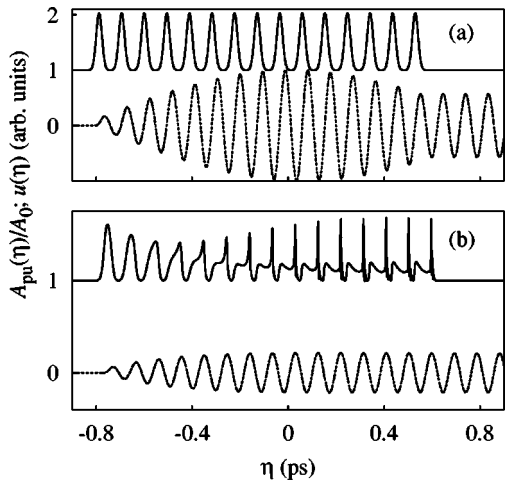

FIG. 18. Envelope of a pump-pulse sequence of 15 20-fs, 20-TW/cm^2, 790-nm pulses (solid line) and Raman excitation (dashed) at the input (a) and at distance $z=1$ m (b) in H_2 at pressure 0.3 atm and for waveguide radius 70 μm.

with separation time T_S and pulse duration $\tau_{pu}<T_R$, can be found from Eq. (27) as follows:

$$u_0=\frac{\sqrt{\pi}\alpha_{12}\tau_{pu}}{4\hbar\sqrt{\ln 2}}A_0^2\exp\left(-\frac{\Omega^2\tau_{pu}^2}{16\ln 2}\right)$$

$$\times\frac{\sin\frac{1}{2}(M+1)\Omega T_S}{\sin\frac{1}{2}\Omega T_S}\cos\frac{1}{2}M\Omega T_S. \qquad (65)$$

If the repetition rate is matched to the rotational or vibrational period $T_S=T_R$, the amplitude of the Raman oscillation u_0 is maximum and for the optimal pump-pulse duration Eq. (37) $u_0=\alpha_{12}A_0^2T_R(M+1)/\sqrt{(8\pi\hbar}$. However, after propagation of a certain distance the Raman polarization induced by the foregoing pulses reacts on the latest pulses and can change their shape and position which in turn re-acts on the polarization and decreases its amplitude.

We studied this problem numerically by the solution of the basic Eqs. (15)–(17) for a sequence of 15 pump pulses, each with intensity of 20 TW/cm^2 and duration of 20 fs at 790 μm and a separation time $T_S=T_R=94$ fs for molecular *para*-H_2 at pressure 0.3 atm and with the Raman polarizability $\alpha_{12}=1.3\times10^{-41}$ Cm^2/V and Sellmeyer coefficients $C_1=0.07$ fs^{-2}, $\omega_1=20.0$ fs^{-1}, $C_2=0.06$ fs^{-2}, and $\omega=25.7$ fs^{-1} [77,78].

In Fig. 18 the envelope of the pump pulses (solid curves) is presented together with the Raman response $u(t)$ (dotted) at the input $z=0$ [Fig. 18(a)] and at distance $z=1$ m [Fig. 18(b). As can be seen, at the input $z=0$ during the first seven pump pulses, the Raman response continuously increases proportionally to the total energy of these pulses. However, the last pulses do not increase the Raman amplitude but lead to a reduction of u_0 due to saturation of the two-level system described by Eqs. (17). The reasonable number of pump pulses is about seven with the total fluence of about 3 J/cm^2, in satisfactory agreement with analytical estimation in Eq. (40). After propagation of 1 m in H_2 the last pulses in Fig. 18(b) are strongly influenced and significantly compressed by the Raman response of the foregoing pump pulses, which leads to short peaks with synchronized repetition time T_R near the maximum of the Raman oscillations and in addition, longer weaker pulses located near the out-of-phase positions. Therefore, u_0 at the output is smaller than at $z=0$ but it reaches a quasisteady state without change during the last pulses due to the opposite action of the short central pulses and the longer intermediate pulses. The decomposition of every individual pulse in case of Fig. 18(b) can be explained by the fact that the Raman response is mainly in phase with the pump pulses itself [see Eq. (27)], therefore every pump pulse is split into two parts with comparable energies as explained by the analytical solution presented in Fig. 5. The action of dispersion leads to compression of one of them and prolongation of the other part. The shorter parts of the pump pulse are located in the maxima of the Raman oscillations, because the positive chirp of the pulses in these positions is compensated by the anomalous dispersion for the redshifted pump pulses. The separation time of the split pulses does not match the Raman period, therefore it interferes, in part, destructively.

Pump-pulse depletion and the splitting of the individual pulses in the train explains the dependence of the Raman amplitude u_0 on the propagation distance and the number of pulses presented by curves 3 and 4 in Fig. 12. The amplification parameter at $z=1$ m for curves 1 and 2 is about $\Gamma\approx2.3$ which is in correspondence with the estimate by Eq. (39). We checked numerically also how accurately the synchronization condition $T_s=T_R$ has to be fulfilled, and found out that a shift of the repetition time by 2% does not influence the excitation remarkably and the pump-pulse synchronism is not destroyed during propagation. In the case of a random change of the repetition time or a jitter the limit for allowed deviations is less severe.

In Fig. 19 we present two examples of probe pulses after propagation through a waveguide filled with *para*-H_2 and pumped by a sequence of 10 pump pulses at 790 nm with duration of 20 fs and intensity of 20 TW/cm^2. The probe pulse at 790 nm [Fig. 19(a,b)] with an initial probe timing in the out-of-phase point is phase modulated after propagation of 1 m through the waveguide [Fig. 19(a)], as can be seen from the spectral phase in [Fig. 19(b)], and has a duration of 4.4 fs. A plate of glass with fitted thickness can compress this pulse to 1.9 fs. The spectral phase of the glass with opposite sign is close to the phase of the pulse in the main part of the spectrum [dashed and thin lines in Fig. 19(b), respectively]. In contrast, a probe pulse at 395 nm [Fig. 19(c,d)] is almost bandwidth-limited after the optimum distance of 65 cm, where the pulse duration is 1.1 fs. The compression here is only due to the dispersion of the gas filling without an additional glass plate. The intensity of the individual pulses in the sequence in Fig. 19 is about the same as in Fig. 15 for pumping by a single pulse. For the probe pulse after the Raman medium we obtained a pulse duration of 11.2 fs which is shortened to 4 fs after a glass plate. In comparison, we see from Fig. 19 that a sequence of ten pump pulses leads to

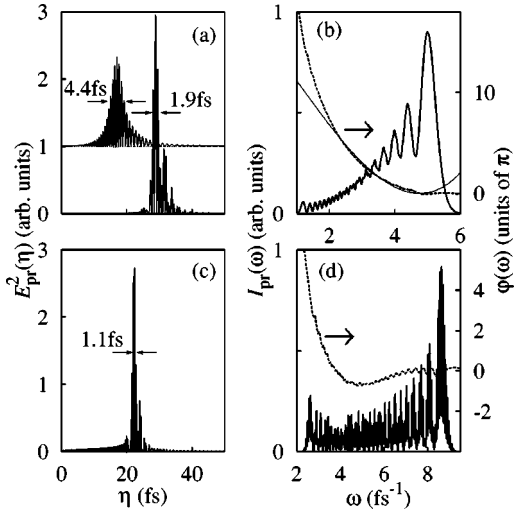

FIG. 19. Temporal (a),(c) and spectral (b),(d) characteristics of the probe pulse for *para*-H_2 at 0.3 atm, pumped by the sequence of ten 20-fs, 20-TW/cm^2, 790-nm pulses and for input pulse of duration 30 fs at 790 (a),(b) and 395 (c),(d) μm. (a) Probe pulse at distance 1 m and after compression by a SiO_2 plate of thickness 54 μm; (b) spectrum (thick line), spectral phase (dashed), and phase of the glass plate (thin); (c) probe pulse at distance 65 cm; and (d) pulse spectrum (thick line) and spectral phase (dashed).

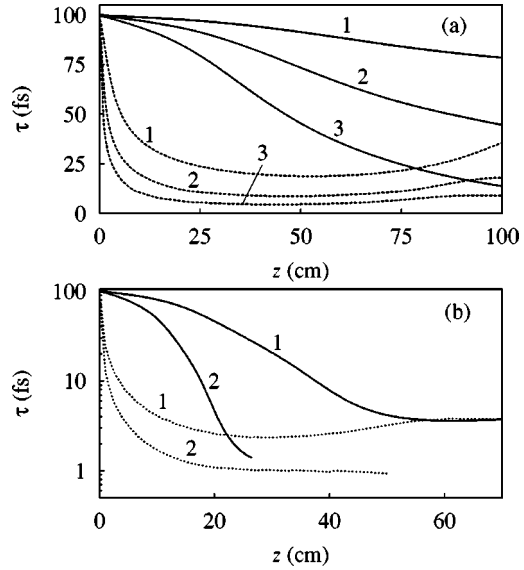

FIG. 20. Probe-pulse duration vs distance (solid curves) and corresponding bandwidth-limited duration (dashed) for input duration 100 fs at 175 nm and for pumping (a) by one 15-TW/cm^2 pulse with duration 90 (1), 70 (2), and 30 fs (3) and (b) by four 20-fs pulses each of intensity 12.5 (1) and 50 TW/cm^2 (2) at 790 nm. Other parameters are as in Fig. 18.

compression to 1.1 fs. This demonstrates the advantage of this pump regime for pulse compression.

V. COMPRESSION OF uv-vuv PULSES

Ultrashort uv-vuv pulses are of great interest for ultrafast time-resolved measurements of atoms, molecules, and solids in physics, chemistry, biology, and material sciences (see, e.g., Refs. [79–81] and references therein). The standard technique to generate ultrashort pulses in the uv-vuv region applies mainly nonlinear optical techniques for frequency conversion. By use of crystalline media with second-order nonlinearity, femtosecond pulse up-conversion has been achieved in wavelengths in the range of 265–166 nm (see, e.g., Refs. [82–84]), but in this method the shortest possible durations are severely limited by walk-off and phase matching limitations. Another method is the use of near-resonant frequency conversion in gases (see, e.g., Refs. [85–89]. Nonresonant frequency conversion by use of gaseous nonlinear media in hollow waveguides with generation of 8 fs at 270 nm has been demonstrated in Ref. [75]. Using cascaded four-wave mixing in hollow waveguides, the generated wavelengths were shifted up to 160–200 nm [90]. However, all methods known up to date suffer from low efficiency or too long pulse durations which are typically in the range of or larger than 100 fs. Therefore, a feasible physical method for pulse compression in uv-vuv would be highly desirable. In the present section we show that pulse compression by HSRS in the pump-probe regime can be extended into the wavelength range of UV/VUV with extremely short output pulses in the range of 1 fs, starting with input probes with a duration of 70–100 fs, which is accessible by the known methods.

The analytical description of uv-vuv pulse compression is identical with that in the optical range given in Sec. III. In difference to the optical region in uv/vuv dispersion has stronger influence and leads to pulse splitting at 1 atm already at short propagation lengths when the spectrum is still not broad enough. This requires one to reduce phase mismatch and walk off by dispersion control of the waveguide, using an optimized pressure. As a result of such optimization we found that for too low a pressure the pulse compression and the spectral broadening is small because of the reduced Raman polarization, while with too high a pressure the bulk contribution to dispersion increases and the effective spectral width remains relatively small because after a certain propagation length pulse splitting occurs.

In Fig. 20(a) the evolution of the duration of a 100-fs, 175-nm input probe pulse with propagation in *para*-H_2 at 0.3 atm and a waveguide radius of 70 μm excited by a single 15-TW/cm^2 pump pulse with different durations is shown. The pulse duration of the same pulses after an ideal compression with exact phase compensation is plotted by dashed lines. The compression is optimum for a pump-pulse duration of about 30 fs; this agrees with the formula for optimum pulse compression given in Eq. (37). As seen in Fig. 20 (a) in curve 3 the ideal compressed pulse has a duration of 4.5 fs. Almost the same result with an output duration of 4.6 fs can be obtained by a real compression using a 90-μm fused silica plate. In order to obtain still shorter pulses one has to realize a higher Raman conversion over a short distance before walk-off effects become critical. As shown in Sec. IV B, a possible way to realize this goal is to use a pump arrangement with synchronized pulse sequences. In Fig. 20(b) the evolution of the pulse duration with propagation in H_2 at 0.3 atm is shown for 100-fs probe pulses with central wave-

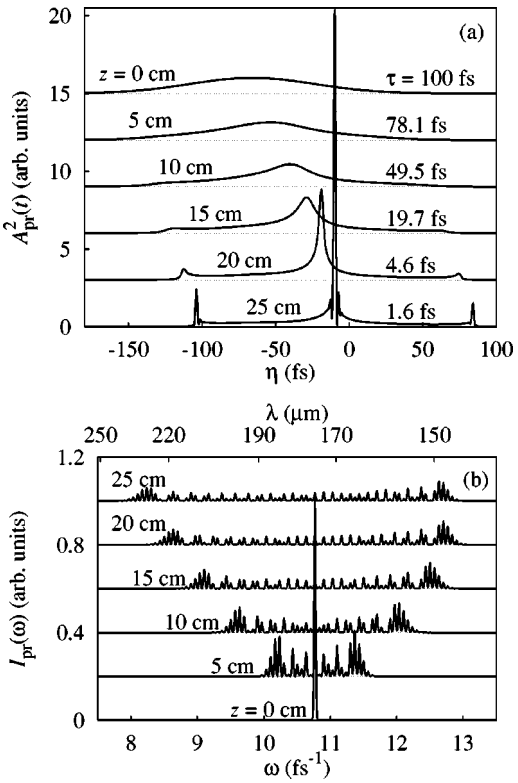

FIG. 21. Evolution of temporal shape (a) and spectrum (b) of 100-fs input-probe pulse at 175 nm for pumping by four 20-fs pulses, each of intensity 50 TW/cm^2 at 790 nm.

length at 175 nm. The waveguide is excited by four 790-nm, 20-fs pump pulses with an intensity of 12.5 TW/cm^2 (curves 1) and 50 TW/cm^2 (curves 2) and a separation time equal the Raman period. The solid lines 2 are interrupted at those lengths where multiple pulses occur due to dispersion.

In Fig. 21 the corresponding evolution of the probe-pulse shape [Fig. 21(a)] and spectrum [Fig. 21(b)] is shown for the the sequence of four synchronized 50-TW/cm^2 pulses. After 25 cm the spectrum is significantly broadened and is extended from 230 nm to 145 nm and the temporal shape shows a compression up to 1.6-fs duration. Note that the probe pulse at distance 25 cm is almost bandwidth limited and the compression occurs due to the normal dispersion of the gas filling only. In Fig. 21(a) two side peaks are formed, temporally shifted from the main pulse by $\pm T_R$, because the input-pulse duration is already in the range of T_R. For a probe input with a duration shorter than about 70 fs such side peaks do not occur.

In Fig. 22 the shape [Fig. 22(a)] and the spectrum [Fig. 22(b)] of a vuv 100-fs pulse at 175 nm are shown for the case of four synchronized pump pulses with the lower intensity of 12.5 TW/cm^2 at distance 25 cm. In this case the spectrum is extended from 160 to 200 nm and the pulse after the Raman medium is compressed to 31.4 fs [curve 1 in Fig. 22(a)] and has a negative chirp as shown by the dashed line in Fig. 22(b). After compression by a plate of SiO_2 with a thickness of 20 μm the probe pulse is compressed to 2.5 fs.

With an increased number of ten pump pulses with only 20-TW/cm^2 intensity, we have predicted compression of

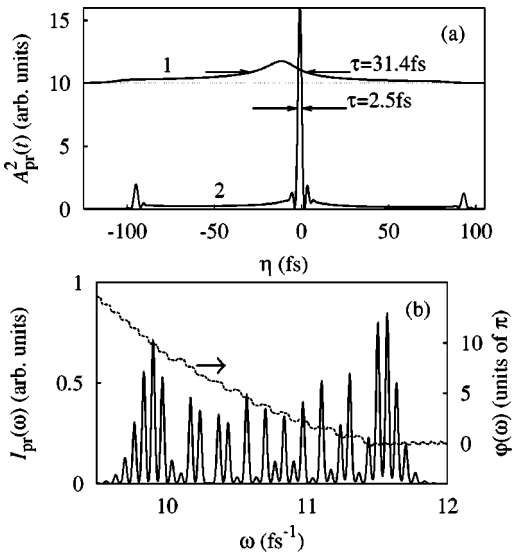

FIG. 22. (a) Temporal shape of a 100-fs, 175-nm vuv pulse after propagation of 25 cm (1) and after compression by 20-μm SiO_2 plate (2), and (b) spectrum and phase of the output probe pulse for pump by four 20-fs pulses of intensity 12.5 TW/cm^2 at 790 nm.

70-fs input probe pulse at 197 nm and 158 nm to 1.28 fs and 1.40 fs, respectively [55]. Thus, the given examples demonstrate the specific features of pulse compression in uv-vuv by HSRS with shortest accessible pulse durations in the range of 1 fs.

Besides pulse compression the enormous bandwidth of the probe pulse after propagation through the hollow waveguide can be used for the generation of tunable uv-vuv pulses with moderate durations. As an example, using simply a spectral filter as, e.g., a multilayered dielectric mirror the spectrum in Fig. 21 can be selected such that without additional chirp compensation bandwidth-limited pulses with a duration of 10–15 fs and central wavelengths tunable from 250 to 150 nm can be generated.

VI. COMPRESSION OF MID-INFRARED PULSES

Ultrashort pulses in the MIR are required for the investigation of elementary physical and chemical processes in condensed matter (see, e.g., Refs. [91–94] and references therein). In most of such studies optical parametric amplification (OPA) is used to generate MIR idler pulses with a typical duration of 100–200 fs. The shortest pulses in MIR at 3–4 μm reported up to now have a duration of about 50 fs, consisting of five cycles (see, e.g., Ref. [95]). Numerous applications demand MIR laser sources with still shorter durations and therefore the development of a feasible pulse compression method for this spectral range is of high importance.

In the present section we show that the method of pulse compression by the application of HSRS has also a great potential in the MIR spectral range. We solve Eqs. (15)–(17) numerically to study the propagation of pump and probe pulses in hollow waveguides filled by molecular *para*-hydrogen with a period of molecular oscillations $T_R = 94$ fs at 1 atm. In Fig. 23 MIR pulse compression is shown for a

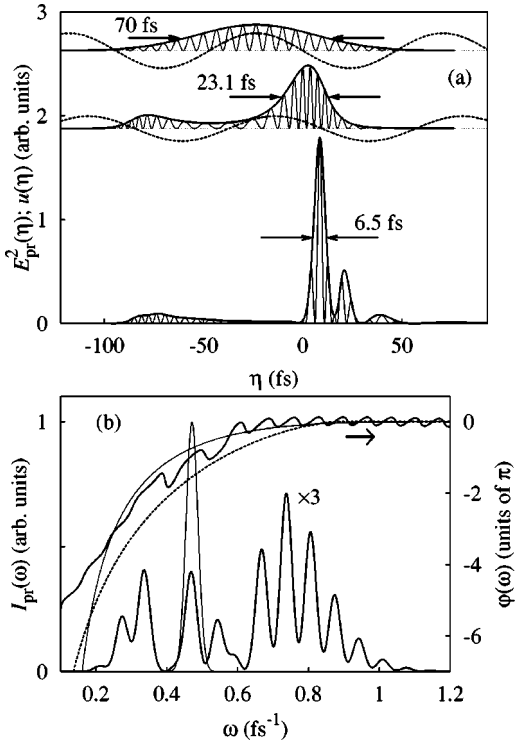

FIG. 23. Temporal (a) and spectral (b) characteristics of a medium infrared pulse in *para*-H_2: (a) From top to bottom, temporal shapes of 70-fs, 4-μm input pulse, output probe pulse at distance 1 m along with Raman oscillations (dashed), and output probe pulse compressed by a 0.3-mm CaF_2 plate; and (b) dotted line, input probe pulse spectrum; thick solid lines, output pulse spectrum and its spectral phase; dashed, the phase of a 0.3-mm CaF_2 plate with opposite sign. Pumping is by a 20-fs, 20-TW/cm^2 pulse at 790 nm, pressure of the molecular H_2 is 1 atm, hollow waveguide radius is 0.5 mm.

20-fs, 20-TW/cm^2 pump pulse at 790 nm. The input probe pulse which can be generated, for instance, by OPA has a duration of $\tau_{pr}=70$ fs at 4 μm. Material dispersion was described by the Sellmeyer formula. The waveguide dispersion plays a special destructive role in the MIR, whereby pulse splitting prevents a compression to short durations. However, with larger waveguide radius $R=0.5$ mm the influence of walk-off effects due to waveguide dispersion can be significantly reduced.

Figure 23(a) presents the input and output probe pulses after propagation of 1 m along with the Raman oscillations. The input pulse was timed to the maximum of Raman oscillations to ensure positive frequency modulation with red frequencies preceding the blue desired for compensation by a piece of glass which typically has anomalous dispersion in the MIR. The output pulse has a double-peaked structure with two maxima in the vicinity of two neighboring out-of-phase points and with an intensity FWHM of 23.1 fs. The spectrum of this pulse is presented in Fig. 23(b), which shows a broadening from 2 to 7.5 μm for a level of 20 dB and with a blue shift of the maximal component to the wavelength 2.5 μm. For comparison the initial spectrum is shown by the thin line. The output spectrum covers almost two octaves, allowing the generation of single-cycle MIR pulses. However, it is not transform limited, as seen in Fig. 23(b), where the spectral phase $\varphi(\omega)$ of the output probe pulse is presented by the solid line. Such kind of phase modulation can be compensated simply by a piece of glass with fitted thickness, which has anomalous dispersion in the MIR. The glass plate may simultaneously serve as an output window of the hollow waveguide and/or as input window of a vacuum chamber where the compressed pulse is used for measurements. The thin line in Fig. 23(b) shows the phase φ_c with opposite sign introduced by a 0.3-mm piece of CaF_2, which is close to the numerically obtained pulse phase $\varphi(\omega)$ so that the residual phase is much less than π in a large part of the whole spectrum. A pulse compressed by the glass plate is presented in Fig. 23(a) (lowest curve), demonstrating the compression to a single-cycle pulse with a FWHM of 6.5 fs, which is unprecedented in the MIR frequency region.

The analytical solution, as given by Eqs. (34) and (35) for the parameter $\Gamma=1.88$, estimated from the numerically calculated amplitude $u_0(z)$ is close to the numerical solution presented in Fig. 23(a), which takes into account the influence of linear dispersion and loss. This shows that for optimized waveguide radius, the influence of the linear dispersion in the MIR on the phase-amplitude modulation is obviously negligible.

The explicit expression (47) for the Fourier-transformed probe field can also be used for the description of the spectrum and spectral phases in MIR. However, for the parameters considered in Fig. 23, two maxima at neighboring out-of phase points occur, therefore in the stationary-phase method both maxima have to be taken into account in the time integral in Eq. (46), which yields the following expression:

$$E_{pr}(\omega)=\frac{C}{\sqrt[3]{\varepsilon\omega}}\{[e^{-i(\omega-\omega_{pr})T_R}A^*_{pr}(s_1-T_R)+A^*_{pr}(s_1)]\mathrm{Ai}(x)+[e^{i(\omega-\omega_{pr})T_R}A_{pr}(s_2-T_R)+A_{pr}(s_2)]\mathrm{Ai}^*(x)\}. \quad (66)$$

Here, $s_{1,2}=t_m\mp\Gamma[(\Gamma\omega_{pr}-\omega)/\varepsilon\omega]^{1/2}$ and other notations are given in Equation (46). Equation (66) predicts all features of the broadened probe spectrum in Fig. 23 for $t_m=-T_R/4$ and gives almost an identical plot (not presented here). For an input peak position $-T_R<t_m<0$, the second term in Eq. (66) dominates and has the spectral phase

$$\varphi(\omega)=-\varphi_a(\omega)=-\frac{2}{3}(\Gamma\omega_0-\omega)^{3/2}/\sqrt{\varepsilon\omega}+\frac{\pi}{4} \quad (67)$$

for $\omega<\Gamma\omega_{pr}$ and $\varphi(\omega)=0$ for $\omega>\Gamma\omega_{pr}$. In Eq. (67) the asymptotics of the Airy function Eqs. (48) and (49) has been used. The phase (67) does not depend on the pulse duration and, as shown in Fig. 23(b) by the dashed line, the difference from the numerically calculated phase caused by the neglect of the first term in Eq. (66) is much less than π.

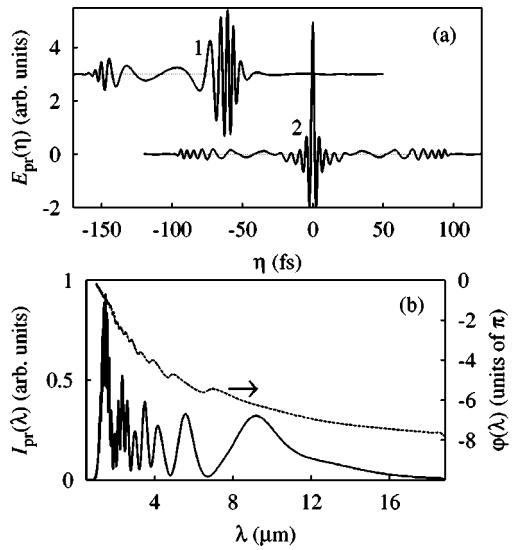

FIG. 24. Temporal shape (a) and spectral characteristics (b) of the MIR probe pulse in *para*-H_2 pumped by four 20-fs, 12.5-TW/cm^2 pump pulses at 790 nm: 1, pulse at distance 1 m with full width at half maximum (FWHM) 12.9 fs; 2, corresponding transformed-limited pulse with FWHM 2.8 fs. Other parameters are as in Fig. 23.

The ultimately shortest pulse duration $\tau_{\min}$, accessible by ideally complete phase compensation, is given by Eq. (51), which predicts rather accurately the duration 6.5 fs of the pulse shown in Fig. 23(a).

We studied also pulse compression of a 50-fs, 4-μm input pulse by *para*-H_2 in the hollow waveguide excited by a synchronized sequence of four 20-fs, 12.5-TW/cm^2 pump pulses at 790 nm (Fig. 24). Curve 1 presents the temporal shape of the pulse with a second weak peak. In Fig. 24(b) the spectrum of the probe pulse after propagation of 1 m is presented, which is extended from about 1 μm to 16 μm, spanning more that four octaves. The spectrum shows several maxima with a peak near 1 μm and a well separated maximum at 10 μm. The spectral phase (dashed line) is close to $-\varphi_a(2\pi c/\lambda)$ given in Eq. (67). The spectral phase of this pulse cannot be compensated simply by a piece of glass, because the dispersion of glass in this spectral range is both normal and anomalous. Curve 2 in Fig. 24(a) shows the pulse shape after ideal phase compensation and demonstrates the generation of a quasi-half-cycle pulse in the MIR spectral region with as short FWHM as 2.8 fs. However, in real experiments such phase compensation by anomalous dispersion from the optical to the MIR spectral region is difficult to realize. On the other hand, if a part of the spectrum in Fig. 24(b) is cut off by a filter, the remaining spectral part is almost bandwidth limited and yields 10–20 fs MIR pulses at tunable central wavelength between 2 and 10 μm. Such short pulses in the MIR have not been generated to date by the known methods.

VII. CONCLUSION

We have reported the results of a comprehensive theoretical study of ultrabroadband phase-amplitude modulation and pulse compression by Raman-active molecular modulators for the impulsive pump-probe regime in spectral ranges reaching from the MIR up to the uv-vuv. Using the analytical solution (34) and (35) without the preposition of SVEA, the simple analytical expressions (42) and (52) were derived for the temporal and spectral characteristics of a probe pulse modulated by the impulsively excited Raman medium, which gives a clear physical understanding of the specific character of pulse compression by HSRS with remarkably different features as compared to SPM. As discussed in Sec. III B, in different regions of the pump-probe delay smooth spectral phases with positive or negative chirp arise, which can be compensated simply by dispersion of a glass plate with normal dispersion in the optical or uv-vuv or anomalous dispersion in the MIR for the generation of extremely short single pulses. Near the out-of-phase position, phase jumps occur within the spectra and in this case a compressor with normal as well with anomalous dispersion decomposes the pulse into a short bandwidth-limited and a long weak phase-modulated part.

To find the optimum waveguide, medium and pump parameters, and the physical limitations for the shortest pulse durations, the influence of dispersion and pump-pulse distortion was studied in different spectral ranges in Secs. IV, V, and VI, respectively, by numerical solutions of the basic equations. It was shown that phase mismatch and walk off due to waveguide and medium dispersion play different roles in different spectral ranges. In the visible region walk off effects are still relatively small for not too large waveguide lengths, while in uv and vuv this effect becomes more critical and leads, in general, to pulse splitting before significant pulse compression can occur. In Sec. V it was shown that the walk-off effect in uv-vuv can be reduced using the waveguide contribution to dispersion with optimized pressure. For a pump intensity just below the ionization threshold the duration of visible or uv-vuv pulses can be decreased to about 2 fs. A possible method to increase the Raman modulation parameter but avoid ionization is the excitation of the Raman medium by a synchronized sequence of pump pulses, which was studied in Secs. IV B and V. Using a sequence of four or ten pulses with a total pulse energy below 0.3 mJ, we have predicted the shortest duration for visible and uv-vuv pulses of about 1 fs. The enormous bandwidth of the probe pulse can also be used for frequency detuning of uv-vuv probe pulse with durations 10–15 fs.

In the MIR spectral range the waveguide contribution to dispersion plays, in general, a crucial destructive role, whereby pulse splitting prevents a compression to short durations. However, for an optimized larger waveguide radius this effect can be significantly reduced. With a probe delay in the range of the maximum of the molecular modulations, the Raman-induced spectral phases of the probe pulse can be compensated by a piece of glass with anomalous dispersion in the MIR. As a result we have found that by a single 20-TW/cm^2 pump pulse, single-cycle MIR pulses with a duration of 6.5 fs can be generated. Using a sequence of four pump pulses, probe pulses with four-octave broad spectra from 1 to 16 μm are predicted and filtered parts of these spectra can be compressed simply by glass plate to tunable

single-cycle pulses. Note that the probe-pulse energy in all spectral ranges can be increased up to relatively high values but still lower than the pump-pulse energy.

Finally, we have shown that pulse compression by HSRS is a feasible physical method to generate extremely short pulses not only in the visible, but also in the MIR and vuv spectral range. A possible experimental realization should have far-reaching applications for time-resolved investigations with an unprecedented time resolution in the spectral ranges from MIR up to vuv and open up new intriguing research in different fields of physics, chemistry, biology, and material science.

ACKNOWLEDGMENT

We acknowledge financial support by the Deutsche Forschungsgemeinschaft.

[1] G. Steinmeyer, D.H. Sutter, L. Gallmann, N. Matuschek, and U. Keller, Science **286**, 1507 (1999).
[2] T. Brabec and F. Krausz, Rev. Mod. Phys. **72**, 545 (2000).
[3] A. Baltuška, Z. Wei, M.S. Pshenichnikov, and D.A. Wiersma, Opt. Lett. **22**, 102 (1997).
[4] M. Nisoli, S. De Silvestri, O. Svelto, R. Szipcs, K. Ferencz, C. Spielmann, S. Sartania, and F. Krausz, Opt. Lett. **22**, 522 (1997).
[5] V.P. Kalosha and J. Herrmann, Phys. Rev. A **62**, 011804 (2000).
[6] A.V. Husakou, V.P. Kalosha, and J. Herrmann, Opt. Lett. **26**, 1022 (2001).
[7] J.J. Macklin, J.D. Kmetec, and C.L. Gordon III, Phys. Rev. Lett. **70**, 766 (1993).
[8] A. L'Huillier and Ph. Balcou, Phys. Rev. Lett. **70**, 774 (1993).
[9] P.B. Corkum, Phys. Rev. Lett. **71**, 1994 (1993).
[10] P. Antoine, A. L'Huillier, and M. Lewenstein, Phys. Rev. Lett. **77**, 1234 (1996).
[11] K.J. Schafer and K.C. Kulander, Phys. Rev. Lett. **78**, 638 (1997).
[12] N.A. Papadogiannis, B. Witzel, C. Kalpouzos, and D. Charalambidis, Phys. Rev. Lett. **83**, 4289 (1999).
[13] I.P. Christov, M.M. Murnane, and H.C. Kapteyn, Phys. Rev. Lett. **78**, 1251 (1997).
[14] P.M. Paul, E.S. Toma, P. Breger, G. Mullot, F. Augé, P. Balcou, H.G. Muller, and P. Agostini, Science **292**, 1689 (2001).
[15] M. Hentschel, R. Kienberger, C. Spielmann, G.A. Reider, N. Milosevic, T. Brabec, P. Corkum, U. Heinzmann, M. Drescher, and F. Krausz, Nature (London) **414**, 509 (2001).
[16] M. Drescher, M. Hentschel, R. Kienberger, M. Uiberacker, V. Yakovlev, A. Scrinzi, Th. Westerwalbesloh, U. Kleineberg, U. Heinzmann, F. Krausz, Nature (London) **419**, 803 (2002).
[17] S.E. Harris and A.V. Sokolov, Phys. Rev. Lett. **81**, 2894 (1998).
[18] A.V. Sokolov, D.R. Walker, D.D. Yavuz, G.Y. Yin, and S.E. Harris, Phys. Rev. Lett. **87**, 033402 (2001).
[19] M. Wittmann, A. Nazarkin, and G. Korn, Phys. Rev. Lett. **84**, 5508 (2000).
[20] M. Wittmann, A. Nazarkin, and G. Korn, Opt. Lett. **26**, 298 (2001).
[21] V.P. Kalosha and J. Herrmann, Phys. Rev. Lett. **85**, 1226 (2000).
[22] V.P. Kalosha and J. Herrmann, Opt. Lett. **26**, 456 (2001).
[23] N. Zhavoronkov and G. Korn, Phys. Rev. Lett. **88**, 203901 (2002).
[24] V. Kalosha, M. Spanner, J. Herrmann, and M. Ivanov, Phys. Rev. Lett. **88**, 103901 (2002).
[25] R.A. Bartels, T.C. Weinacht, N. Wagner, M. Baertschy, C.H. Greene, M.M. Murnane, and H.C. Kapteyn, Phys. Rev. Lett. **88**, 013903 (2002).
[26] A.V. Sokolov, D.R. Walker, D.D. Yavuz, G.Y. Yin, and S.E. Harris, Phys. Rev. Lett. **85**, 562 (2000).
[27] F. LeKien, J.Q. Liang, M. Katsuragawa, K. Ohtsuki, K. Hakuta, and A.V. Sokolov, Phys. Rev. A **60**, 1562 (1999).
[28] N.H. Shon, F. LeKien, K. Hakuta, and A.V. Sokolov, Phys. Rev. A **65**, 033809 (2002).
[29] F. LeKien, N.H. Shon, and K. Hakuta, Phys. Rev. A **64**, 051803 (2001).
[30] F. LeKien, K. Hakuta, and A.V. Sokolov, Phys. Rev. A **66**, 023813 (2002).
[31] F. LeKien, K. Hakuta, and A.V. Sokolov, Phys. Rev. A **66**, 055802 (2002).
[32] S. Yoshikawa and T. Imasaka, Opt. Commun. **96**, 94 (1993).
[33] A.E. Kaplan, Phys. Rev. Lett. **73**, 1243 (1994).
[34] Z. Sheng, J. Ma, and W. Yu, J. Opt. Soc. Am. B **10**, 122 (1993).
[35] Y.R. Shen, *The Principles of Nonlinear Optics* (Wiley, New York, 1984).
[36] W. Kaiser and M. Maier, in *Laser Handbook*, edited by F.T. Arecchi and E.O. Schultz-Dubois (North-Holand, Amsterdam, 1972).
[37] V. Schulz-von der Garten, T. Bornemann, V. Kornas, and H.F. Döbele, IEEE J. Quantum Electron. **26**, 739 (1990).
[38] Y.-X. Yan, E.B. Gamble, and K.A. Nelson, J. Chem. Phys. **83**, 5391 (1985).
[39] S. Ruhman, A. Joly, and K. Nelson, IEEE J. Quantum Electron. **34**, 460 (1988).
[40] A.M. Weiner, D.E. Leaird, G.P. Wiederrecht, and K.A. Nelson, J. Opt. Soc. Am. B **8**, 1264 (1991).
[41] R.W. Turhune, Solid State Design **4**, 38 (1963).
[42] R.Y. Chiao and B.P. Stoicheff, Phys. Rev. Lett. **12**, 290 (1964).
[43] D. Eimerl, D. Milam, and J. Yu, Phys. Rev. Lett. **70**, 2738 (1993).
[44] H. Kawano, Y. Hirakawa, and T. Imasaka, IEEE J. Quantum Electron. **34**, 260 (1998).
[45] V. Krylov, O. Ollikainen, U.P. Wild, A. Rebane, V.G. Bespalov, and D.I. Staselko, J. Opt. Soc. Am. B **15**, 2910 (1998).
[46] H. Kawano, T. Mori, Y. Hirakawa, and T. Imasaka, Phys. Rev. A **59**, 4703 (1999).
[47] J.Q. Liang, M. Katsuragawa, F. LeeKien, and K. Hakuta, Phys. Rev. Lett. **85**, 2474 (2000).

[48] K. Ishikawa, H. Kawano, and K. Midorikawa, Phys. Rev. A **66**, 031802 (2002).
[49] A.P. Hickman, J.A. Paisner, and W.K. Bischel, Phys. Rev. A **33**, 1788 (1986).
[50] A.P. Hickman and W.K. Bischel, Phys. Rev. A **37**, 2516 (1988).
[51] L.L. Losev and A.P. Lutsenko, Kvant. Elektron. (Moscow) **20**, 1054 (1993).
[52] G.S. McDonald, G.H.C. New, L.L. Losev, A.P. Lutsenko, and M. Shaw, Opt. Lett. **19**, 1400 (1994).
[53] A. Nazarkin, G. Korn, M. Wittmann, and T. Elsaesser, Phys. Rev. Lett. **83**, 2560 (1999).
[54] A. Nazarkin, G. Korn, M. Wittmann, and T. Elsaesser, Phys. Rev. A **65**, 041802 (2002).
[55] V.P. Kalosha and J. Herrmann, Phys. Rev. A **67**, 031801 (2003).
[56] V.P. Kalosha and J. Herrmann, Opt. Lett. **28**, 950 (2003).
[57] K.S. Yee, IEEE Trans. Antennas Propag. **14**, 302 (1966).
[58] R.W. Ziolkowski, J.M. Arnold, and D.M. Gogny, Phys. Rev. A **52**, 3082 (1995).
[59] V.P. Kalosha and J. Herrmann, Phys. Rev. Lett. **83**, 544 (1999).
[60] R.K. Bullough, P.M. Jack, P.W. Kitchenside, R. Saunders, Phys. Scr. **20**, 364 (1979).
[61] A.V. Husakou and J. Herrmann, Phys. Rev. Lett. **87**, 203901 (2001).
[62] M. Born and E. Wolf, *Principles of Optics* (Pergamon Press, New York, 1989).
[63] W.H. Press, A.A. Teukolsky, W.T. Vetterling, and B.P. Flannery, *Numerical Recipes in Fortran* (Cambridge University Press, Cambridge, 1992).
[64] J.E. Rothenberg, Opt. Lett. **17**, 1340 (1992).
[65] S. Chi and Q. Guo, Opt. Lett. **20**, 1598 (1995).
[66] G. Fibich and B. Ilan, Phys. D **157**, 112 (2001).
[67] A.V. Husakou and J. Herrmann, J. Opt. Soc. Am. B **19**, 2171 (2002).
[68] M. Nisoli, S. De Silvestri, and O. Svelto, Appl. Phys. Lett. **68**, 2793 (1996).
[69] E.A.J. Marcatili and R.A. Schmeltzer, Bell Syst. Tech. J. **43**, 1783 (1964).
[70] V.S. Butylkin, A.E. Kaplan, Y.G. Khronopulo, and E.I. Yakubovich, *Resonant Nonlinear Interactions of Light with Matter* (Springer-Verlag, New York, 1977).
[71] V.I. Smirnov, *Course of Higher Mathematics* (Pergamon Press, Oxford, 1964).
[72] *Handbook of Mathematical Functions*, edited by M. Abramowitz and I.A. Stegun (Dover Publications, New York, 1972).
[73] J.A. Gardecki, S. Constantine, Y. Zhou, and L.D. Ziegler, J. Opt. Soc. Am. B **17**, 652 (2000).
[74] S. Yeremenko, A. Baltuška, F. de Haan, M.S. Pshenichnikov, and D.A. Wiersma, Opt. Lett. **27**, 1171 (2002).
[75] C.G. Durfee, S. Backus, H.C. Kapteyn, and M.M. Murnane, Opt. Lett. **24**, 697 (1999).
[76] *Gmelin Handbuch der Anorganischen Chemie*, edited by H. Bitterer (Springer-Verlag, Berlin, 1978).
[77] *Raman Spectroscopy of Gases and Liquids*, edited by A. Weber (Springer-Verlag, Berlin, 1979).
[78] See Ref. [46] and references therein.
[79] A.H. Zewail, *Femtochemistry-Ultrafast Dynamics of Chemical Bonds* (World Scientific, Singapore, 1994).
[80] P. Farmanara, O. Steinkellner, M.T. Wick, M. Wittmann, G. Korn, V. Stert, and W. Radloff, J. Chem. Phys. **111**, 6264 (1999).
[81] J.M. Mestdagh, J.P. Visticot, M. Elhanine, and B. Soep, J. Chem. Phys. **113**, 237 (2000).
[82] J. Ringling, O. Kittelmann, F. Noack, G. Korn, and J.A. Squier, Opt. Lett. **18**, 2035 (1993).
[83] A. Dubietis, G. Tamošauskas, A. Varanavičius, G. Valiulis, and R. Danielius, Opt. Lett. **25**, 1116 (2000).
[84] V. Petrov, F. Rotermund, F. Noack, J. Ringling, and R. Komatsu, IEEE J. Sel. Top. Quantum Electron. **5**, 1532 (1999).
[85] A. Tünnermann, C. Momma, K. Mossavi, C. Windolph, and B. Wellegehausen, IEEE J. Quantum Electron. **29**, 1233 (1993).
[86] B. Wellegehausen, H. Welling, C. Momma, M. Feuerhake, K. Mossavi, and H. Eichmann, Opt. Quantum Electron. **38**, 267 (1996).
[87] J.H. Glownia, D.R. Gnass, and P.P. Sorokin, J. Opt. Soc. Am. B **11**, 2427 (1994).
[88] O. Kittelmann, J. Ringling, G. Korn, A. Nazarkin, and I.V. Hertel, Opt. Lett. **21**, 1159 (1996).
[89] M. Wittmann, M.T. Wick, O. Steinkellner, P. Farmanara, V. Stert, W. Radloff, G. Korn, and I.V. Hertel, Opt. Commun. **173**, 323 (2000).
[90] L. Misoguti, S. Backus, C.G. Durfee, R. Bartels, M.M. Murnane, and H.C. Kapteyn, Phys. Rev. Lett. **87**, 013601 (2001).
[91] C. Chudoba, E.T.J. Nibbering, and T. Elsaesser, Phys. Rev. Lett. **81**, 3010 (1998).
[92] G.M. Gale, G. Gallot, F. Hache, N. Lascoux, S. Bratos, and J.-C. Leickman, Phys. Rev. Lett. **82**, 1068 (1999).
[93] R. Laenen, T. Roth, and A. Laubereau, Phys. Rev. Lett. **85**, 50 (2000).
[94] J. Stenger, D. Madsen, P. Hamm, E.T.J. Nibbering, and T. Elsaesser, Phys. Rev. Lett. **87**, 027401 (2001).
[95] V. Petrov, F. Rotermund, and F. Noack, J. Opt. A, Pure Appl. Opt. **3**, 1 (2001).